2021

A Novel Method for Analysis of Proprioceptor Sensory Neuron Subtypes in the Mouse Dorsal Root Ganglia

Delaney C. Grant
Wright State University

A NOVEL METHOD FOR ANALYSIS OF PROPRIOCEPTOR SENSORY NEURON SUBTYPES IN THE MOUSE DORSAL ROOT GANGLIA

A thesis submitted in partial fulfillment of the
requirements for the degree of
Master of Science

By

DELANEY C. GRANT
B.S., University of Cincinnati, 2019

2021
Wright State University

WRIGHT STATE UNIVERSITY

GRADUATE SCHOOL

April 28, 2021

I HEREBY RECOMMEND THAT THE THESIS PREPARED UNDER MY SUPERVISION BY Delaney C. Grant ENTITLED A Novel Method for Analysis of Proprioceptor Sensory Neuron Subtypes in the Mouse Dorsal Root Ganglia BE ACCEPTED IN PARTIAL FULFILLMENT OF THE REQUIREMENTS FOR THE DEGREE OF Master of Science.

David R. Ladle, Ph.D.
Thesis Director

Eric S. Bennett, Ph.D.
Department Chair
Department of Neuroscience, Cell Biology and Physiology

Committee on
Final Examination

David R. Ladle, Ph.D.

Patrick M. Sonner, Ph.D.

Mark M. Rich, M.D., Ph.D.

Barry Milligan, Ph.D.
Vice Provost for Academic Affairs
Dean of the Graduate School

ABSTRACT

Grant, Delaney C. M.S. Department of Neuroscience, Cell Biology and Physiology, Wright State University, 2021. A Novel Method for Analysis of Proprioceptor Sensory Neuron Subtypes in the Mouse Dorsal Root Ganglia.

Proprioceptive sensory neurons encode critical mechanosensory information that helps determine how the body interacts with the outside world and monitors the proper execution of motor movements. Housed in skeletal muscles lie specialized mechanoreceptors that are critical to this feedback loop: muscle spindles supplied by group Ia & group II afferents, and Golgi tendon organs supplied by group Ib afferents relay information regarding changes in muscle force, length, and tension. All three afferent subtypes originate in the muscle and travel to the dorsal root ganglia, relaying information to the central nervous system. GTO and MS proprioceptive afferent subtypes have been identified, traced, and labeled by restrictive RNA and DNA sequencing techniques that eliminate the potential for *in vivo* and *ex vivo* analysis. To confirm the identity of different proprioceptive afferent subtypes in the dorsal root ganglia of mice, the present study developed a method of fluorescence tracing using a dextran dye to trace afferents and their origins. By injecting tetramethylrhodamine dextran dye directly into the quadriceps muscle, the muscle spindle proprioceptive afferents selectively transport the dye to the cell body in the DRG demonstrating its origin and classification. Being able to selectively label and trace muscle spindle afferents allows us to accurately collect data on the cells in the DRGs.

TABLE OF CONTENTS

Page

LISTS OF FIGURES

Figure Page

LISTS OF TABLES

Table Page

I. Introduction

Proprioception

One of the most crucial aspects of human survival is interacting with and moving around the environment. An integral part of this function is the proprioceptive sense, an entity's perception of the body's movements and orientation in 3D space. Nerves travel from the neuromuscular junction to the spinal cord and inform the central nervous systems of all muscle movements. This information is interpreted by the cerebrum and confirms the execution of motor tasks and muscle movements. Understanding this complex circuit allows for the development of treatments for diseases and injuries affecting proprioception, like recovery after peripheral nerve injury.

Proprioceptive feedback is dependent mainly on specialized mechanoreceptive organs in the skeletal muscle. These proprioceptive afferents relay critical feedback to the central nervous system regarding the successful completion of motor tasks. Sensory afferents from the skin, muscle, and joints provide necessary information regarding alterations in muscle length, force, stretch, and joint angles to the spinal cord and central nervous system (Sherrington, 1907; Windhorst, 2007). Proprioceptive sensory neurons (pSNs) are comprised of specialized mechanoreceptors that originate in skeletal muscles and project their cell bodies to the dorsal root ganglia (DRG) beside the spinal cord, connecting to the central nervous system

(Matthews, 1964). Extensive physiological studies have identified two distinct mechanoreceptor subtypes: muscle spindles (MSs) supplied by group Ia and group II afferents and Golgi tendon organs (GTOs) supplied by group Ib afferents (Matthews, 1964; Schoultz and J.E., 1972; Granit, 1975). Information from both MS and GTO afferents is relayed to higher brain centers via projections through the dorsal spinocerebellar tract (DSCT) and ventral spinocerebellar tract (VSCT) (Oscarsson, 1965; Shrestha et al., 2012). Together these proprioceptive sensory neuron inputs are responsible for conveying information pertaining to the state of muscle activation and movement to the central nervous system, mainly through monosynaptic connections with specific motor neurons (Baldissera et al., 1981; Poliak et al., 2016).

Muscle Spindle Afferents

The muscle spindle has been an area of interest for over a century, originating when Sherrington first categorized the muscle spindle as a sense organ (Sherrington, 1884). Muscle spindle (MS) mechanoreceptors are hyaluronic acid-filled capsules embedded in the belly of skeletal muscles and in parallel with extrafusal muscle fibers (De-doncker et al., 2003; Banks, 2005). MS afferents are approximately 6-10mm long and structurally complex, consisting of a bundle of intrafusal muscle fibers of several different types (bag 1, bag 2, and chain fibers) surrounded by a capsule (Matthews,

1964; Banks et al., 1982; Hunt and Louis, 1990). Each muscle fiber has an equatorial region devoid of myofibrils and containing nuclei with two contractile poles (De-doncker et al., 2003). The largest muscle fibers, nuclear bag fibers 1 and 2, have a significant accumulation of nuclei in the equatorial region of the sarcomeric structure and are approximately 20-25 μm in diameter (Hunt and Louis, 1990). Nuclear bag fiber 1 and nuclear bag fiber 2 are distinguished by their histochemical attributes, and the bag 1 fiber is usually slightly longer than the bag 2 fiber (Hunt and Louis, 1990). Nuclear chain fibers are approximately 10-12 μm in diameter (De-doncker et al., 2003) and are usually much shorter than nuclear bag fibers (Hunt and Louis, 1990). They typically run the entire length of the spindle and show a collection of nuclei in linear formation in the fiber's equatorial region (Hunt and Louis, 1990).

These encapsulated intrafusal muscle fibers are innervated by one primary (group Ia axons), several secondary (group II axons) afferents, and gamma motor neuron axons. (Matthews, 1964; Banks et al., 1982; Sonner et al., 2017). The primary ending is the largest sensory axon to the muscle spindle and contacts each intrafusal muscle fiber, and also displays extensive annulospiral terminations in their nucleated regions (Boyd, 1962; Hunt and Louis, 1990). In contrast, the smaller group II afferents primarily contact intrafusal chain fibers and have flower-spray endings (Boyd, 1962; Banks et

al., 1982; Hunt and Louis, 1990; Sonner et al., 2017). While both primary and secondary endings respond to stretch, their distinct endings encode stimuli differently.

During a ramp-and-hold stretch, Ia afferents and II afferents exhibit different firing responses (Crowe and Matthews, 1964). Most notably, during ramp stretch, Ia afferents exhibit firing frequencies that depend upon the velocity of the stretch that is higher than at the static level and paused during the stretch release (Hunt and Louis, 1990; De-doncker et al., 2003). Group II afferents show little dynamic responses during ramp stretch, but instead exhibit linear responses with muscle length and responses gradually increase to static level (Hunt and Louis, 1990; De-doncker et al., 2003). Additionally, group Ia afferents showed a higher sensitivity to vibration frequencies than group II afferents (De-doncker et al., 2003). As a result, group II afferents encode static stretch and group Ia afferents encode information regarding the dynamic stretch, also known as changes in velocity (Matthews, 1981).

Golgi Tendon Organ Afferents

Like the muscle spindle, Golgi tendon organs (GTOs) are specialized mechanoreceptors critical to the successful execution of motor tasks. Golgi tendon organs (GTOs), supplied by group Ib afferents, are encapsulated stretch-activated proprioceptive sensory afferents found in the skeletal muscle that respond to change in muscle load and tension (Schoultz and J.E., 1972;

Jami, 1992). One main difference between the two structures is the GTO afferents reside in the myotendinous junction of the skeletal muscle and respond to distinctly different stimuli (muscle load and tension) (Scott, 2005). GTO afferents are encapsulated sensory nerve endings positioned in series with extrafusal muscle fibers that they innervate, allowing them to be highly sensitive to rapid changes in contractile force while responding little to stretch (Houk and Henneman, 1967; Davies et al., 1995). Typically, a GTO is supplied by a single large-diameter myelinated Ib afferent, which has extensive branches and is closely associated with collagen strands (Schoultz and J.E., 1972). Though GTO and MS afferents are integral parts of the proprioceptive sense, they are distinct structures with various physiological properties and functions.

Development and Reinnervation

While proprioceptive sensory neurons' physiology and their targets are well understood, comprehending their development and reinnervation after an injury has evolved significantly in recent years. MS and GTO afferents selectively innervate their central and peripheral targets, but proprioceptor physiology can be altered after peripheral nerve injury (PNI). Problems with recovery after PNI can result in poor motor control and sensation (Verdu and Navarro, 1997). Understanding the underlying methods of proprioceptor

reinnervation is essential to develop improved therapies to aid in recovery after PNI.

During normal proprioceptive nerve development, proprioceptor sensory neuron progenitors are born from day e9.5 to day e10 in the first wave of DRG sensory neurogenesis and are initially segregated into two distinct genetic lineages: $TrkB^{+}Shox2^{+}$ and $TrkC^{+}Rx3^{+}$ (Ma et al., 1999; Kramer et al., 2006; Lallemend and Ernfors, 2012; Wu et al., 2019). Rapidly adapting low threshold mechanoreceptors (RA-LTMRs) develop from $TrkB^{+}Shox2^{+}$ progenitor cells (Abdo et al., 2011; Li et al., 2011), while the $TrkC^{+}Rx3^{+}$ lineage gives rise to slowly adapting low threshold mechanoreceptors (SA-LTMRs) and to proprioceptive muscle afferents (de Nooij et al., 2013; Wu et al., 2019). Around day e14.5, proprioceptive sensory afferents mark their commitment to the pSN lineage by expression of parvalbumin (PV) (Tourtellotte and Milbrandt, 1998; Hippenmeyer et al., 2002; Wu et al., 2019). It has been shown that proprioceptor subtypes development depends upon extrinsic sensory receptor organ-derived signals (Wu et al., 2019) and intrinsic inductive signals for innervating sensory axons (Hippenmeyer et al., 2002). After PNI, regenerating neurons express post-injury gene programs, including the expression of embryonic and developmental genes, both of which contribute to axonal regrowth and regeneration (Blackmore, 2012; Hilton and Bradke, 2017).

After PNI, axons in peripheral nerves maintain the capacity to regenerate and reinnervate, providing potential for functional recovery and improved prognosis (Verdu and Navarro, 1997; Chandran et al., 2016). Functional recovery after PNI entails regrowth of injured axons and reinnervation of the muscle and target tissues, but this process is often incomplete due to complications (Barker et al., 1985; He and Jin, 2016; Renthal et al., 2020). The ability of axons to regrow and reinnervate properly depends upon the type and severity of the injury. Two main models of PNI in rodent models are sciatic nerve crush and sciatic nerve transection, and both have well-established reinnervation and regrowth time courses (Brown and Butler, 1976; Collins et al., 1986; Dun and Parkinson, 2018). However, various complications and post-injury alterations impact the proprioceptive sensory neuron's ability to reinnervate their target muscle and resume normal physiological functions.

Approximately 50% of proprioceptive afferents fail to reconnect and reinnervate the correct muscle spindles after peripheral nerve injury, specifically in transection injuries (Banks et al., 1982). Also, proprioceptive afferents exhibit abnormal or decreased firing rates in response to muscle manipulation (Collins et al., 1986). Additional challenges in PNI recovery include morphological alteration to proprioceptive sensory neuron afferents and non-specific reinnervation of target tissues. Following reinnervation of

muscle spindles after nerve crush, some group Ia afferents were shorter than normal and exhibited fewer transverse bands, and some group II afferents showed signs of growth through the primary ending region (Collins et al., 1986). While the majority of sensory axons reinnervate the correct target tissue after PNI, there is evidence that regenerating proprioceptive afferents may misconnect to the wrong target tissue (Banks et al., 1982). In-depth investigation of pSN reinnervation and regeneration is limited by the ability to selectively identify and isolate subtype-specific pSN afferents, particularly MS afferents from GTO afferents. Distinguishing between MS and GTO afferents, specifically at the DRG level, allows for confirmation of subtype identity while investigating gene expression during development and after injury.

Labeling and Identification

Currently, the main method of classifying and distinguishing subtype-specific afferents has relied on various genetic strategies (Wu et al., 2019; Oliver et al., 2021). RNA sequencing technology allows for the identification of molecularly distinct neuronal clusters and gene expression profiling (Wu et al., 2019; Oliver et al., 2021). While this technology allows for specific distinction between neuronal subtypes, RNA sequencing is not applicable to living preparations used during electrophysiological experiments. Previous studies have used retrograde tracers to track axons and presynaptic structures

and map out projection patterns of neurons (Kamiyama et al., 2015; Odagaki et al., 2018). Intracutaneous injection of Alexa488-conjugated (and 549-conjugated CTB) has shown to be effective at labeling cutaneous afferent projections from the forelimbs of mice to the dorsal horn of the spinal cord (Odagaki et al., 2018). *In vivo* injection of a retrograde tracer (green fluorescent latex microspheres) has successfully labeled brain and spinal cord tissue without fading or diffusion, permitting the analysis of spinal circuits during development (Katz et al., 1984; Katz and Iarovici, 1990; Kamiyama et al., 2015).

While there are various studies that utilize retrograde tracers in brain tissue and spinal tissue, there is a lack of knowledge surrounding the application of retrograde tracers in muscle to label neurons in the DRG (Katz et al., 1984; Katz and Iarovici, 1990; Blumer et al., 2003; Odagaki et al., 2018). The technique employed in this project utilized a dextran dye, tetramethylrhodamine (rhodamine), and injected it directly into the rectus femoris (quadriceps) muscle of mice. This project rests on the hypothesis that injecting rhodamine dye into the muscle selectively labels muscle spindle afferents due to their location in the belly of the muscle, where the dye is transported to the cell bodies in the corresponding DRGs; conversely, Golgi tendon organ afferents are not labeled due to their location at the myotendinous junctions. To confirm the selective uptake of rhodamine dye by

muscle spindles, DRGs were sectioned and stained to confirm the presence of double labeled cells. While the results of this experiment are preliminary, the procedure and method of selectively labeling MS afferents in the DRG has many applications. For example, it could be used to confirm the proprioceptor subtype during reinnervation and after PNI.

II. Materials and Methods

Animals

All animal experiments were approved by the Wright State University Institutional Animal Care and Use Committee and conducted following the guidelines set by the National Institute of Health. Wild-type mice (C57BL/6J) were used for all experiments.

Mice that did not undergo surgery were used for the *ex vivo* rhodamine muscle injection experiments and the *ex vivo* sciatic nerve backfill experiments. Three mice aged P4 to P10 were used for the *ex vivo* rhodamine muscle injection experiments (labeled mouse 1, mouse 2, and mouse 3), and four mice aged P5 to P7 were used for the *ex vivo* sciatic nerve backfill experiments (labeled mouse 1, mouse 2, mouse 3, and mouse 4). Two mice, one male (mouse 6A) and one female (mouse 6B), aged P23, were used for the *in vivo* rhodamine muscle injection experiments. These mice underwent surgery as described below. All procedures were conducted in accordance with Wright State University Institutional Animal Care and Use Committee. After 24 hours, mouse 6B was euthanized via 0.03 mL intraperitoneal injection of Euthasol and dissected as described below. Mouse 6A was euthanized after 48 hours via 0.03 mL intraperitoneal injection of Euthasol and dissected as described below.

Tissue Preparation

Mice were anesthetized using an intraperitoneal Euthasol injection (older than P7) or by induction of hypothermia (younger than P7). In a dissecting chamber, mice were transcardially perfused with 5mL of ice-cold oxygenated (5% CO2; 95% O2) artificial cerebrospinal fluid (ACSF) containing 127 mM NaCl, 1.9 mM KCL, 1.2 mM KH_2PO_4, 1 mM $MgSO_47H_2O$, 26 mM $NaHCO_3$, 2 mM $CaCl_2$, and 16.9 mM D(+)-glucose monohydrate. Animals were then decapitated, and the vertebral column (from T1) was isolated along with the hips and legs. Dissections were performed in a dissecting dish with the animal preparation fully submerged in a bath of circulating cold ACSF. After the procedures were performed, as described below, animal tissue was fixed with 4% cold paraformaldehyde (PFA) solution for 24 hours. Animal preparation was then washed with 1X Phosphate buffer solution (PBS) twice and equilibrated with 30% sucrose solution (in PBS) for 24 hours for cryoprotection. Animal preparation is dissected to isolate the structure of interest (DRGs or muscles), and structures are individually embedded in Tissue Tek O.C.T. compound and frozen at -80˚C. Using a cryostat (Thermo-Fisher Scientific), tissue was sectioned in 20 μm increments and transferred to Fisherbrand Superfrost Plus Microscope Slides. Immunohistochemistry was performed on every fifth section, as described below.

A. Ex Vivo Rhodamine Muscle Injection

After mice were euthanized, transcardially perfused, and transferred to an ACSF bath, as previously described, the right and left femoral nerve and quadriceps muscles were identified and isolated. Tetramethylrhodamine dye was injected parallel to the direction of the muscle fibers and into the right and left rectus femoris via a glass micropipette. After 12 hours of remaining in the dissection dish with circulating room temperature ACSF, the animal preparation was fixed with 4% PFA as described above. Animal preparation was washed with PBS, equilibrated with 30% sucrose, embedded, frozen, and sectioned as described above. Before embedding, the right and left rectus femoris muscles are isolated. To ensure the inclusion of Golgi tendon organ afferents, which are located in the tendons connected to the muscle, the patella distal to the rectus femoris is included in the tissue sample embedded. After sectioning, immunohistochemistry was performed on every fifth section, and slides were coverslipped using Vectashield mounting medium to preserve fluorescence signals prior to imaging and coverslips were added for image analysis.

B. Ex Vivo Sciatic Nerve Backfills

Mice aged P5 to P7 were used for the sciatic nerve backfill experiments. Starting at approximately T1, the spinal cord was exposed by

performing a dorsal laminectomy, and the dura was removed to allow for better circulation of ACSF to the DRGs. Excess dorsal muscles were dissected, and preparation was flipped to the ventral side, and extra abdominal trunk muscles were removed. The left leg was removed, and on the dorsal side, the posterior biceps semi tendinosis (PBST) nerve is transected, and additional muscle superficial muscles were removed. The sural, peroneal, and tibial nerves were identified and cut, and the hipbone was removed to expose the sciatic nerve. To achieve better oxygenation of the spinal cord and DRG's, the thoracic portion of the spinal cord was dissected from the vertebral column. The femur and tibia/fibula were removed to expose the sciatic nerve fully.

A glass micropipette was pulled, fire-polished to fit the sciatic nerve diameter to ensure a proper suction fit. The sciatic nerve was cut, and the glass micropipette was fitted around the end of the sciatic nerve using a micromanipulator. The micropipette was loaded with tetramethylrhodamine dye (approximately 1.5 μL). After 12 hours of remaining in the dissection dish with circulating room temperature ACSF, the animal preparation was fixed, washed with PBS, and equilibrated with 30% sucrose as previously described.

Animal preparation was further dissected to isolate the target DRG's (L4, L5, and L6). The vertebral column was transected superior to the L4

DRG and inferior to L6. To easily quickly the labeled side, the L6 DRG was removed from the unlabeled side. The spinal column was embedded and frozen before sectioning. After sectioning, immunohistochemistry was performed as described below, and slides were coverslipped using Vectashield mounting medium to preserve fluorescence signals prior to imaging and coverslips were added for image analysis.

C. In Vivo Rhodamine Muscle Injections

One male and one female mouse, both P21, were anesthetized using isoflurane (3.4-5%) in a chamber and subsequently transferred to a sterile drape where a nose cone was fitted over the animal's head to administer the isoflurane continuously. With sterile instruments, a 3-4 mm incision in the upper right thigh on each mouse's ventral side was made to gain access to the rectus femoris muscle. The incision was extended through the fascia, and through this incision, tetramethylrhodamine (rhodamine) dye was injected into the rectus femoris muscle using a glass micropipette and the assistance of a microscope. The micropipette was positioned so that the micropipette needle was parallel to the muscle fibers in the rectus femoris muscle and on the distal end of the muscle. Approximately 2 to 3 injections were administered to allow the rectus femoris muscle to be completely and evenly labeled. The incision was closed using 6-0 USP silk sutures, and an analgesic was applied to the incision site.

Mouse 6B and 6A followed the same protocols, except mouse 6B was euthanized after 24 hours of survival, and mouse 6A was euthanized after 48 hours of survival. Mice were euthanized via an intraperitoneal injection of 0.03 mL Euthisol and transcardially with 5mL cold 1X PBS, and subsequently, through the same injection site, 10mL of cold 4% PFA was perfused. The spinal cord and legs were isolated as described before. A dorsal laminectomy was performed to allow for better access to the spinal cord and circulation of ACSF to the DRGs, and the dura was removed. The animal preparation was then fixed in 4% PFS, washed with PBS, and equilibrated with 30% sucrose as described previously. The L4, L5, and L6 DRGs were isolated by transecting superior to the L4 vertebrae and inferior to the L6 vertebrae before embedding. Only the right quadriceps muscles were embedded since it was the target of the injections. After embedding in Tissue Tek O.C.T. compound in a Peel-A-Way chamber, the tissue was frozen and cut at 20 μm as previously described.

Immunohistochemistry

Immunohistochemistry was performed on 20 μm sections. All slides were washed three times with 1X PBS for 5 minutes each time. Slides were incubated in a primary antibody solution (1X PBS solution with 1% bovine serum albumin and 0.3% Triton X-100) overnight at 4˚C.

Primary antibodies used differed depending on the tissue being stained. For muscle tissue, primary antibodies included guinea pig anti- vGLUT1 polyclonal antibody diluted 1:10,000 (Chemicon AB5905, Lot LV1567574) and rabbit anti-tetramethylrhodamine polyclonal antibody diluted 1:5,000 (Life Tech A6397, Lot 1476653). Primary antibodies used for the analysis of the DRGs included rabbit anti tetramethylrhodamine polyclonal antibody diluted 1:5,000 (Life Tech A6397, Lot 1476653) and goat anti parvalbumin polyclonal antibody diluted 1:10,000 (Swant PVG-214 Lot 3.6).

The next day slides were washed 3 times with 1X PBS for 5 minutes each. Slides were incubated in a secondary antibody solution (1X PBS solution with 1% bovine serum albumin and 0.3% Triton X-100) for 45 minutes at 22˚C. Secondary antibodies varied depending on the tissue. For muscle tissue, antibodies used were donkey anti guinea pig Alexa 488 polyclonal antibody diluted 1:500 (Jackson IR J 706-545-148, Lot 118980) and donkey anti-rabbit Cy3 polyclonal antibody diluted 1:500 (Jackson IR J 711-165-152, Lot 120991). For DRG tissue, secondary antibodies included donkey anti-goat Alexa488 polyclonal antibody diluted 1:500 (Invitrogen A11055), and donkey anti-rabbit Cy3 polyclonal antibody diluted 1:500 (Jackson IR J 711-165-152, Lot 120991). Following the secondary antibody solution's incubation, the slides were washed 3 times with 1X PBS for 5 minutes each. Slides were coverslipped using Vectashield mounting medium to preserve fluorescence

signals prior to imaging and coverslips were added for image analysis. Analysis of slides is described below.

Analysis of Lumbar DRG

L3, L4, and L5 DRG sections were analyzed for the quadriceps *in vivo* rhodamine muscle injection experiments, and L4, L5, and L6 DRG sections were analyzed for the *ex vivo* sciatic nerve backfill experiments. Slides were analyzed using an Olympus BX51 Epi-fluorescence microscope and Olympus cellSense Software. Pictures of DRGs were taken in both the FITC (green) and TRITC (red) channels and combined channels. Three different types of cells were recorded in each DRG: parvalbumin-expressing (PV+) cells, Rhodamine expressing cells (Rhod+), and double-positive cells (PV+/Rhod+). PV+ cells fluoresced green and were counted as positive if the cells were bright green, significantly above the background. Rhod+ cells fluoresced bright red, and cells were considered positive if they fluoresced in the red channel above the background. Double positive cells express both PV and Rhodamine, and the cells fluoresce green and red significantly above the background.

The number of cells was counted in each labeled DRG (the DRGs that were ipsilateral to the nerve/tissue labeled with the rhodamine dye) using ImageJ software and Cell Counter plug-in. The amount of PV+, Rhod+, and double-labeled cells were recorded in Excel. To accurately assess each cell

type's distribution, the total number of PV+, Rhod+, and double-labeled cells in each DRG (and across all animals) was counted and compared to the percent of total labeled cells in that specific DRG. The number of each cell type was averaged between animals and compared to the total number of cells. Example images of the L4, L5, and L6 DRGs from the sciatic nerve backfill experiments and images of the L3, L4, and L5 DRGs from the *in vivo* rhodamine muscle injection experiments were obtained using an Olympus FV1000 confocal microscope. Images were then analyzed using Fluoview software (Olympus FV10-ASW Version 4.2 B).

Analysis of Quadriceps Muscle

Slides were initially analyzed using an Olympus BX51 Epi-fluorescence microscope to record the location and number of each proprioceptor afferents (MSs and GTOs) on each section. Muscle spindles were identified by distinguishing morphological characteristics, specifically the annulospiral structures around muscle fibers and flower-spray morphology. GTO afferents were found at the myotendinous junction and identified by their highly branched endings. More detailed images of the sensory neuron afferent were acquired using an Olympus FV1000 confocal microscope (10X and 20X objectives used). MS and GTO afferent images were analyzed using Fluoview software (Olympus FV10-ASW Version 4.2B). Muscle spindle afferents were analyzed based on three characteristics: if they were double-labeled (the

muscle spindle afferent appears in both Alexa 488 channel and Cy3 channel), if they were located in an area where the surrounding muscle is labeled with the rhodamine dye, and if the intrafusal muscle fibers the MS was wrapped around fluoresced red (signaling that it had taken up the rhodamine dye). GTO afferents were analyzed based on the following characteristics: if the GTO was double-labeled, meaning it fluoresced in the Alexa488 channel and the Cy3 channel, and if the GTO was located net to or near muscle fibers that had taken up the rhodamine dye and fluoresced red.

To assess the distribution of rhodamine dye and the association of MS afferents with the dye, the percent of MSs associated with Rhod+ muscle fibers was quantified and compared to the percent of MSs located in an area where the surrounding muscle fibers had taken up the dye. Mouse 1, mouse 2, and mouse 3 were compared in the *ex vivo* rhodamine muscle injection experiments, and mouse 6B and mouse 6A were compared in the *in vivo* rhodamine muscle injection experiments.

III. Results

Ex Vivo Rhodamine Muscle Injections

Initial microscopy analysis showed an even and thorough distribution of rhodamine dye among the muscle fibers of the rectus femoris muscle, both right and left. There were three mice used: one P6 (labeled mouse 1), one P5 (labeled mouse 2), and one P3 (labeled mouse 3). Table 1 displays a summary of data from mouse 1, mouse 2, and mouse 3 analyzed to confirm the success of the *ex vivo* rhodamine injections into the quadriceps muscle. Since no muscle spindles were truly double-labeled (fluorescing in both the vGLUT1 channel and rhodamine channel equally), the quality of rhodamine dye distribution in the muscle and the association of proprioceptive afferents (MSs and GTOs) was quantified in two different ways: whether the proprioceptive afferent (for muscle spindles and Golgi tendon organs) were located in an area where the surrounding muscle was labeled with rhodamine, and if the proprioceptive afferent (muscle spindles only) was associated with a red muscle fiber.

For mouse 1 there were 10 slides analyzes, and of those slides, 64 sections were analyzed. There was a total of 10 sections that contained proprioceptive structures (either MS or GTO afferents). Overall, mouse 1 had 14 MS afferents and no GTO afferents. Of the 14 total MS afferents analyzed, 11 were wrapped around a muscle fiber labeled with rhodamine dye (78.6%), and 14 were located in an area where the surrounding muscle was dyed with rhodamine (100%).

Mouse 2 had 6 slides analyzed with a total of 24 sections, and of those, 10 sections contained proprioceptive structures (MSs or GTOs). A total of 9 muscle spindle afferents and 6 GTO afferents were identified. Of the muscle spindles analyzed, 8 of them were associated with a rhodamine-dyed fiber (88.9%), and 8 of them resided in an area where the surrounding muscle fiber was rhodamine-labeled (88.9%). The muscle sections obtained from Mouse 2 displayed 6 GTO afferents, and of those, only 1 was located near muscle fibers that were rhodamine-labeled (approximately 16.67%).

Of the three mice analyzed, Mouse 3 had the most proprioceptive afferents, with 5 GTO afferents and 22 MS afferents visible. Of the muscle spindles examined, 18 of the 22 were associated with a rhodamine-labeled muscle fiber (82%), and all 22 spindles were located in an area where the surrounding muscle had an even distribution of rhodamine dye (100%). Contrastingly, only 40% of GTO afferents (2 out of 5) were located near muscle fibers labeled with rhodamine dye.

In summary, a total number of 45 muscle spindles and 11 Golgi tendon organs were analyzed. Of the muscle spindles examined, 37 of them (82.2%) were wrapped around a muscle fiber that fluoresced red, confirming the uptake of rhodamine dye in that fiber (Figure 2). Although not every MS analyzed was associated with a red muscle fiber (8 were not), almost all muscle spindles (44 spindles; 98% of all spindles) were in an area of muscle where there was an even distribution of rhodamine dye in the surrounding muscle (Figure 2). These results indicate that the *ex vivo* rhodamine muscle injections

were only partly successful. Even though the rhodamine dye showed an even distribution in the rectus femoris muscle, the muscle spindles were not double-labeled and therefore did not take up the rhodamine dye. However, no GTO afferents were double-labeled, and only a small percentage of them were located near rhodamine dyed tissues.

Ex Vivo Sciatic Nerve Backfills

Another goal of this project was to confirm the transport of rhodamine dye from proprioceptive nerve afferents to the supporting DRGs. Fire-polished micropipettes were suctioned around sciatic nerves in the *ex vivo* mouse preparation procedure previously mentioned, and rhodamine dye was backfilled into the pipette on top of the open end of the sciatic nerve. To assess the successful uptake of the rhodamine dye, specifically by proprioceptive afferents, immunohistochemistry was utilized to label PV+ cells. Parvalbumin (PV) is a well-known molecular marker for proprioceptive neurons in DRGs, specifically MS and GTO sensory neurons (Arber et al., 2000). Immunohistochemistry was also used to label Rhod+ cells in the DRG, afferents that took up the rhodamine dye from the sciatic nerve. PV+ cells in the DRG are proprioceptor afferents that project to the sciatic nerve, and these cells fluoresced green. Cells that fluoresced red were cells that expressed rhodamine (Rhod+); therefore, cells that only fluoresced green (PV+ cells) were proprioceptive neurons that did not originate from the sciatic nerve and therefore did not take up the rhodamine dye. Rhod+ cells in the DRG (cells that fluoresced only red) are neurons that originate in the sciatic nerve that are not

proprioceptors. Double-labeled cells that fluoresced both red and green (PV+/Rhod+) are proprioceptive neurons that originate in the sciatic nerve and took up the rhodamine dye.

To assess the successful transport of the rhodamine dye by proprioceptive sensory neurons, the number of PV+, Rhod+, and double-labeled cells were counted in the L4, L5, and L6 DRG (Table 2). For this experiment, four mice were used (mouse 1, mouse 2, mouse3, and mouse 4). On average, the L4 DRG exhibited 56.67 ± 49.97 PV+ cells, 3.33 ± 5.77 Rhod+ cells, and 23.33 ± 32.62 double-labeled (Figure 7C). Mouse 1 only had 6 labeled cells, and mouse 3 did not have any visible L4 DRGs (Table 2). The majority of labeled cells in the L4 DRG were proprioceptors that did not originate from the sciatic nerve, with 68% of cells being PV+ cells. Rhod+ cells only represented 4% of the total population of labeled cells, and 28% of labeled cells were double-labeled (Figure 7B). The L4 DRG had the least number of labeled cells, with the majority of labeled cells being non-sciatic proprioceptors (PV+) and sciatic proprioceptors (double-labeled cells).

The L5 DRG had considerably more double-labeled cells, with 59.08% of labeled cells displaying both red and green fluorescence and an average number of 95 ±120.26 double-labeled cells. (Figure 8A). A total of 400 PV+/Rhod+ cells were observed across four animals and 14 sections (Table 2). On average, there were 14.50 ± 10.79 Rhod+ cells and 54.75 ± 48.36 PV+ cells in the L5 DRG. Of the proprioceptors labeled (cells labeled by PV) in the L5 DRG, the majority of cells (64.6%) project to the sciatic nerve. The remaining proprioceptors (35.4%) project to other nerves and only fluoresce green

(PV+). From this data, it can be concluded that the majority of PV+ proprioceptors projecting to the sciatic nerve (PV+/Rhod+) originate in the L5 DRG, but there is also a small population of Rhod+ cells and a considerable amount of PV+ cells (Figure 10).

The L6 DRG exhibited an average of 38.73 ± 27.03 PV+ cells, 7.50 ± 15 Rhod+ cells, and 41.75 ± 54.91 double-labeled cells (Figure 9C). There were almost equal amounts of PV+ and double-labeled cells, with 155 cells and 167 cells, respectively (Figure 9A and 9B). On average, the L6 DRG had 7.5 ± 15 Rhod+ cells, cells that project to the sciatic nerve but are not proprioceptive neurons (Figure 9C). The L6 DRG showed, on average, more labeled cells than the L4 DRG but less labeled cells than the L5 DRG (Figure 10).

These results indicate that proprioceptive nerve afferents can transport rhodamine dye to the DRG and effectively labeling pSNs in the mouse DRGs. Overall, the majority of rhodamine labeled proprioceptive afferents that project to the sciatic nerve were located in the L5 DRG (Figure 10). The L5 DRG contained the most labeled cells, with the L6 DRG having less and the L4 DRG having the least number of labeled cells. Even though the experiments were successful, there was considerable variability between animals, contributing to large standard deviation values. More accurate data could be obtained by adding additional trials.

In Vivo Rhodamine Muscle Injections

A. Muscle Analysis

Initial analysis of MS afferents showed an even and complete distribution of the rhodamine dye in the rectus femoris muscle of both mouse 6A and mouse 6B, mainly in the belly of the muscle where the MSs are located (Figure 11). Of the MS afferent observed, 91.3% of them in mouse 6B and 77.78% were associated with red muscle fibers that took up the rhodamine dye (Figure 13). Further analysis using confocal microscopy revealed that 69.57% of MSs imaged in mouse 6B and 66.67% of MSs imaged in mouse 6B were located in an area with thorough rhodamine distribution. 39.13% of muscle spindles in Mouse 6B were double-labeled, and one-third of MSs (33.33%) in mouse 6A were double-labeled. Of all three categories analyzed, mouse 6A had slightly fewer double-labeled muscle spindles and less rhodamine dye distribution than mouse 6B (Figure 13). This could be partially due to the differences in survival times, as mouse 6A survived for 48 hours post injection and mouse 6B survived for 24 hours post-injection. To confirm this, however, there would need to be a larger sample size from both groups.

Unfortunately, only 5 GTOs were able to be identified between mouse 6A and mouse 6B. Most of the GTOs imaged were not located near the rhodamine dye (Figure 12). None of the 3 GTOs imaged from mouse 6A or the 2 GTOs imaged from mouse 6B were double-labeled. Only 1 GTO (from mouse 6A) was located in an area where the muscle had taken up the rhodamine dye. While the sample size is small, this data shows that GTOs are likely not labeled by the rhodamine dye.

B. DRG Analysis

To better assess the effectiveness of the rhodamine dye labeling proprioceptive afferents in the DRG, the L3, L4, and L5 DRG on the ipsilateral side (right side) of the injected muscle were analyzed. Unfortunately, both mouse 6A and mouse 6B preparations did not yield many visible cells in the DRGs. However, some identifiable cells were present in the L3, L4, and L5 DRGs (Figure 15). The L3 DRG in mouse 6B displayed 25 PV+ cells, 1 Rhod+ cell, and 41 PV+/Rhod+ (double-labeled) cells, while mouse 6A only had 9 PV+ cells, no Rhod+ cells and 5 double-labeled cells in the L3 DRG. On average, the L3 DRG exhibited 17 ± 11.31 PV+ cells, 0.5 ± 0.71 Rhod+ cells, and 23 ± 25.45 double-labeled cells (Figure 18 C).

In mouse 6B, there were fewer labeled cells in the L4 DRG than in the L3 DRG; however, in mouse 6A there were more labeled cells in the L4 DRG than in the L3 DRG (Figure 21). The L4 DRGs varied in the number of each cell types depending on the mouse (6B vs. 6A). The L4 DRG in mouse 6B displayed 23 PV+ cells, 1 Rhod+ cell, and 19 double-labeled cells (Figure 19A). Conversely, mouse 6A had 32 PV+ cells, 1 Rhod+ cell, and 6 double-labeled cells (Figure 19A). On average, the L4 DRG contained 27.5 ± 6.36 PV+ cells, 1 ± 0 Rhod+ cells, 12.5 ± 9.19 double-labeled cells, and 41 ± 2.83 total labeled cells (Figure 19C). Compared to the L4 DRGs in the *ex vivo* sciatic nerve backfill, the L4 DRGs from the *in vivo* rhodamine muscle injection experiments displayed fewer labeled cells. On average, the L4 DRGs from the *ex vivo* experiments

displayed a total of 83.33 ± 67.34 labeled cells; and the L4 DRGs from the *in vivo* experiments had an average of 41 ± 2.83 labeled cells. However, it is essential to note that the *ex vivo* experiments labeled cells from the sciatic nerve and the *in vivo* experiments labeled cells originating in the rectus femoris muscle and projecting to the spinal cord via the femoral nerve, so there are various elements to consider when comparing the two.

The L5 DRG in both mouse 6B and mouse 6A displayed very few labeled cells. Despite this, some double-labeled cells were present in mouse 6A and 6B, and one Rhod+ cell in the L5 DRG of mouse 6A (Figure 20A). Mouse 6B had 14 PV+ cells and 8 double-labeled cells, while mouse 6A exhibited 12 PV+ cells, no Rhod+ cells, and 10 double-labeled cells (Figure 20A). The L5 DRG had an average of 13 ± 1.41 PV+ cells, no Rhod+ cells, and 9 ± 1.41 double-labeled cells (Figure 20C). Similar to the L4 DRGs, the L5 DRGs from the *in vivo* rhodamine muscle injection experiments exhibited fewer cells than the L5 DRGs from the *ex vivo* sciatic nerve backfill experiments. The L5 DRGs from the *ex vivo* experiments had an average of 88 ± 79.27 total labeled cells, while the L5 DRGs from the *in vivo* experiments had an average of 22.0 ± 0 labeled cells.

Mouse 6B, which had a survival time of 24 hours post-surgery, displayed more labeled cells than mouse 6A, which had a survival time of 48 hours. Fluorescence microscopy showed that mouse 6B had a total of 150 labeled cells consisting of 62 PV+ cells, 2 Rhod+ cells, and 68 double-positive cells, with the majority of them (67 cells)

residing in the L3 DRG (Figure 21A). Mouse 6A had 75 labeled cells comprising of 53 PV+ cells, 1 Rhod+ cell, and 21 double-labeled cells, where the L4 DRG had the most labeled cells (39 cells) (Figure 21B). From this data, it can be concluded that the mouse 6B preparation was more successful at labeling cells in the DRGs than the mouse 6A preparation. Due to the limitation of the small sample size (n=1 in each group), no confident comparison can be made between the two post-surgery survival times.

.

Percent of Muscle Spindles Associated with Rhodamine Dye Distribution						
	# of MSs double-labeled	# of MSs with Assocaiated Fiber Red	# of MSs with Surrounding Muscle Red	Total Number of MSs	% of MSs with Associated Fiber Red	% of MSs with Surrounding Muscle Red
Mouse 1	0.00	11.00	14.00	14.00	0.79	1.00
Mouse 2	0.00	8.00	8.00	9.00	0.89	0.89
Mouse 3	0.00	18.00	22.00	22.00	0.82	1.00
Average	**0.00**	12.33	14.66	15.00	0.83	0.96

Golgi Tendon Organ Association with Rhodamine Dye				
	# of GTOs double-labeled	GTOs Located Near Rhodamine Dyed Tissue	Total number of GTOs	% of GTOs Near Rhodamine Dye
Mouse 1	0.00	0.00	0.00	0.00
Mouse 2	0.00	1.00	6.00	0.17
Mouse 3	0.00	2.00	5.00	0.40
Average	0.00	2.33	3.66	0.19

Table 1: *Ex Vivo* Muscle Injection: Rhodamine Distribution in Relation to MS and GTO Location. Between mouse 1, mouse 2, and mouse 3, there was an average of 15 muscle spindles per mouse, and an average of 83% of those was associated with a rhodamine-dyed (red) fiber, and 96% of them were located in an area where the surrounding muscle. Each animal had an average of 1 GTO imaged, and on average, 19% of GTOs are located in an area where Rhodamine dye is present in the surrounding tissue.

Analysis of Ex Vivo Sciatic Backfill DRG: L4, L5, and L6						
Slide	Section	Location	PV+ Cells (Green Cells)	Rhod+ Cells (Red Cells)	PV+/Rhod+ Cells (Double-Labeled)	Total Number of cells
Mouse 1 1-A	1	L6	7	0	8	15
Mouse 1 2-A	1	L4	2	0	4	6
Mouse 1 2-A	1	L5	4	6	31	41
Mouse 1 2-A	1	L6	14	0	12	26
Mouse 2 1-A	5	L4	18	0	14	32
Mouse 2 1-A	7	L4	17	0	7	24
Mouse 2 1-A	8	L4	9	0	15	24
Mouse 2 1-A	5	L5	27	2	36	65
Mouse 2 1-A	7	L5	10	2	22	34
Mouse 2 1-A	8	L5	17	1	27	45
Mouse 2 1-A	5	L6	19	0	2	21
Mouse 2 1-A	7	L6	7	0	0	7
Mouse 2 2-A	1	L4	11	0	0	11
Mouse 2 2-A	1	L4	13	0	25	38
Mouse 2 2-A	2	L5	8	0	6	14
Mouse 3 1-A	1	L5	17	5	44	66
Mouse 3 1-A	2	L5	21	0	64	85
Mouse 3 1-A	3	L5	31	3	49	83
Mouse 3 1-A	4	L5	23	12	37	72
Mouse 3 1-A	5	L5	14	6	42	62
Mouse 3 1-A	6	L5	12	1	35	48
Mouse 3 1-A	1	L6	15	0	34	49
Mouse 3 1-A	2	L6	14	0	28	42
Mouse 3 1-A	3	L6	18	0	24	42
Mouse 3 1-A	4	L6	15	0	19	34
Mouse 3 1-A	5	L6	17	0	18	35
Mouse 4 1-A	4	L4	31	2	0	33
Mouse 4 1-A	5	L5	8	8	4	20
Mouse 4 1-A	6	L4	22	5	0	27
Mouse 4 1-A	6	L5	5	6	0	11
Mouse 4 1-A	6	L6	11	11	11	33
Mouse 4 1-A	7	L5	22	6	3	31
Mouse 4 1-A	7	L6	9	5	5	19
Mouse 4 1-A	8	L6	9	14	6	29
Mouse 4 1-B	3	L4	12	0	0	12
Mouse 4 1-B	4	L4	32	1	4	37
Mouse 4 1-B	5	L4	3	2	1	6
TOTAL			**544**	**98**	**637**	**1279**

Table 2: *Ex Vivo* Sciatic Nerve Backfills: Number of Cells Labeled. Distribution of cells in the L4, L5, and L6 DRGs across mouse 1, mouse 2, mouse 3, and mouse 4.

Number of Cells in L4, L5, and L6 DRG		
Analysis of Labeled Cells in L4 DRG		
	# of Cells	**% of Total Cells**
PV+ Cells	170	68.00%
Rhod+ Cells	10	4.00%
PV+/Rhod+ Cells	70	28.00%
Analysis of Labeled Cells in L5 DRG		
	# of Cells	**% of Total Cells**
PV+ Cells	219	32.35%
Rhod+ Cells	58	8.57%
PV+/Rhod+ Cells	400	59.08%
Analysis of Labeled Cells in L6 DRG		
	# of Cells	**% of Total Cells**
PV+ Cells	155	44.03%
Rhod+ Cells	30	8.52%
PV+/Rhod+ Cells	167	47.44%

Table 3: *Ex Vivo* Sciatic Nerve Backfills: Individual Lumbar DRG Analysis. Comparison of the number and distribution of labeled cells in the L4, L5, and L6 DRG.

Average Number of Cells in L4, L5, and L6 DRG				
Average # of Cells in L4 DRG				
Animal #	PV+ (Green Cells)	Rhod+ (Red Cells)	PV+/Rhod+ (Double Labeled Cells)	Total Number of cells
Mouse 1	2	0	4	6
Mouse 2	68	0	61	129
Mouse 4	100	10	5	115
Average # of Cells	**56.67**	**3.33**	**23.33**	**83.33**
Average # of Cells in L5 DRG				
Animal #	PV+ (Green Cells)	Rhod+ (Red Cells)	PV+/Rhod+ (Double Labeled Cells)	Total Number of cells
Mouse 1	4	6	31	41
Mouse 2	62	5	71	138
Mouse 3	118	27	271	416
Mouse 4	35	20	7	62
Average # of Cells	**54.75**	**14.50**	**95.00**	**164.25**
Average # of Cells in L6 DRG				
Animal #	PV+ (Green Cells)	Rhod+ (Red Cells)	PV+/Rhod+ (Double Labeled Cells)	Total Number of cells
Mouse 1	21	0	20	41
Mouse 2	26	0	2	28
Mouse 3	79	0	123	202
Mouse 4	29	30	22	81
Average # of Cells	**38.75**	**7.50**	**41.75**	**88.00**

Table 4: *Ex Vivo* Sciatic Nerve Backfills: Average Number of Cells in L4, L5, and L6 DRGs. The total number of each cell type from mouse 1, mouse 2 mouse 3, and mouse 4 was averaged to reflect the numbers of labeled cells in the average mouse L4, L5, and L6 DRGs.

In Vivo Rhodamine Muscle Injection: MS Afferent Analysis				
Animal	Number of MS with Associated Muscle Fiber Red	Number of MS with Surrounding Fiber Red	Total Number of MS Afferents Identified	Number of Double Labeled MS Afferents
Mouse 6B	21	16	23	9
Mouse 6A	7	6	9	3
	Percent of MS afferents with Associated Fiber Red	Percent of MS Afferents with Surrounding Fiber Red	Percent of MS Fibers that are Double Labeled	
Mouse 6B	91.30%	69.57%	39.13%	
Mouse 6A	77.78%	66.67%	33.33%	
Average	84.54%	68.12%	36.23%	
***In Vivo* Rhodamine Muscle Injection: GTO Afferent Analysis**				
Animal	Number of GTO Afferents Located Near Red Muscle Fibers	Number of GTO Afferents Double Labeled	Total Number of GTO Afferents	
Mouse 6B	0	0	2	
Mouse 6A	1	0	3	
	Percent of GTO Afferents Located Near Red Muscle Fibers		Percent of GTO Afferents Double Labeled	
Mouse 6B	0%		0%	
Mouse 6A	33.33%		0%	
Average	16.67%		0%	

Table 5: *In Vivo* Rhodamine Muscle Injection: GTO and MS Afferent analysis. In both mouse 6A and 6B, the majority of muscle spindles imaged were associated with muscle fibers that absorbed the rhodamine dye. However, all but one GTO imaged was not associated with the rhodamine dye.

Analysis of cells in Mouse 6B L3 DRG						
Slide	Section	Location	PV+ (Green Cells)	Rhod+ (Red Cells)	PV+/Rhod+ (Double Labeled)	Total Number of cells
Mouse 6B 1-B	5	L3	0	0	7	7
Mouse 6B 1-B	10	L3	4	0	6	10
Mouse 6B 2-B	2	L3	7	0	10	17
Mouse 6B 2-B	3	L3	8	1	9	18
Mouse 6B 2-B	4	L3	5	0	6	11
Mouse 6B 2-B	5	L3	1	0	3	4
TOTAL			**25**	**1**	**41**	**67**
Analysis of cells in Mouse 6B L4 DRG						
Slide	Section	Location	PV+ (Green Cells)	Rhod+ (Red Cells)	PV+/Rhod+ (Double Labeled)	Total Number of cells
Mouse 6B 1-B	10	L4	0	0	5	5
Mouse 6B 2-B	2	L4	3	0	3	6
Mouse 6B 2-B	3	L4	6	0	4	10
Mouse 6B 2-B	4	L4	13	0	4	17
Mouse 6B 2-B	5	L4	1	1	3	5
TOTAL			**23**	**1**	**19**	**43**
Analysis of cells in Mouse 6B L5 DRG						
Slide	Section	Location	PV+ (Green Cells)	Rhod+ (Red Cells)	PV+/Rhod+ (Double Labeled)	Total Number of cells
Mouse 6B 1-B	10	L5	7	0	4	11
Mouse 6B 2-B	4	L5	3	0	4	7
Mouse 6B 2-B	11	L5	4	0	0	4
TOTAL			**14**	**0**	**8**	**22**
Total Cell Count for Mouse 6B						
Animal		PV+ (Green Cells)	Rhod+ (Red Cells)	PV+/Rhod+ (Double Labeled)	Total Number of cells	
Mouse 6B		**62**	**2**	**68**	**132**	

Table 6: *In Vivo* Rhodamine Muscle Injection: Cell Count for Mouse 6B. Distribution of labeled cells across L3, L4, and L5 DRGs.

Analysis of cells in Mouse 6A L3 DRG						
Slide	Section	Location	PV+ (Green Cells)	Rhod+ (Red Cells)	PV+/Rhod+ (Double Labeled)	Total Number of cells
Mouse 6A 2-B	1	L3	1	0	1	2
Mouse 6A 2-B	2	L3	5	0	2	7
Mouse 6A 2-B	3	L3	0	0	0	0
Mouse 6A 2-B	4	L3	2	0	2	4
Mouse 6A 2-B	5	L3	1	0	0	1
TOTAL			**9**	**0**	**5**	**14**
Analysis of cells in Mouse 6A L4 DRG						
Slide	Section	Location	PV+ (Green Cells)	Rhod+ (Red Cells)	PV+/Rhod+ (Double Labeled)	Total Number of cells
Mouse 6A 2-B	1	L4	8	0	0	8
Mouse 6A 2-B	2	L4	4	0	1	5
Mouse 6A 2-B	3	L4	11	0	0	11
Mouse 6A 2-B	4	L4	3	1	1	5
Mouse 6A 2-B	5	L4	6	0	4	10
TOTAL			**32**	**1**	**6**	**39**
Analysis of cells in Mouse 6A L5 DRG						
Slide	Section	Location	PV+ (Green Cells)	Rhod+ (Red Cells)	PV+/Rhod+ (Double Labeled)	Total Number of cells
Mouse 6A 2-B	1	L5	3	0	0	3
Mouse 6A 2-B	2	L5	0	0	2	2
Mouse 6A 2-B	3	L5	5	0	1	6
Mouse 6A 2-B	4	L5	1	0	7	8
Mouse 6A 2-B	5	L5	3	0	0	3
TOTAL			**12**	**0**	**10**	**22**
Total Cell Count for Mouse 6A						
Animal		PV+ (Green Cells)	Rhod+ (Red Cells)	PV+/Rhod+ (Double Labeled)	Total Number of cells	
Mouse 6A		**53**	**1**	**21**	**75**	

Table 7: *In Vivo* Rhodamine Muscle Injection: Cell Count for Mouse 6A. Distribution of labeled cells across L3, L4, and L5 DRGs.

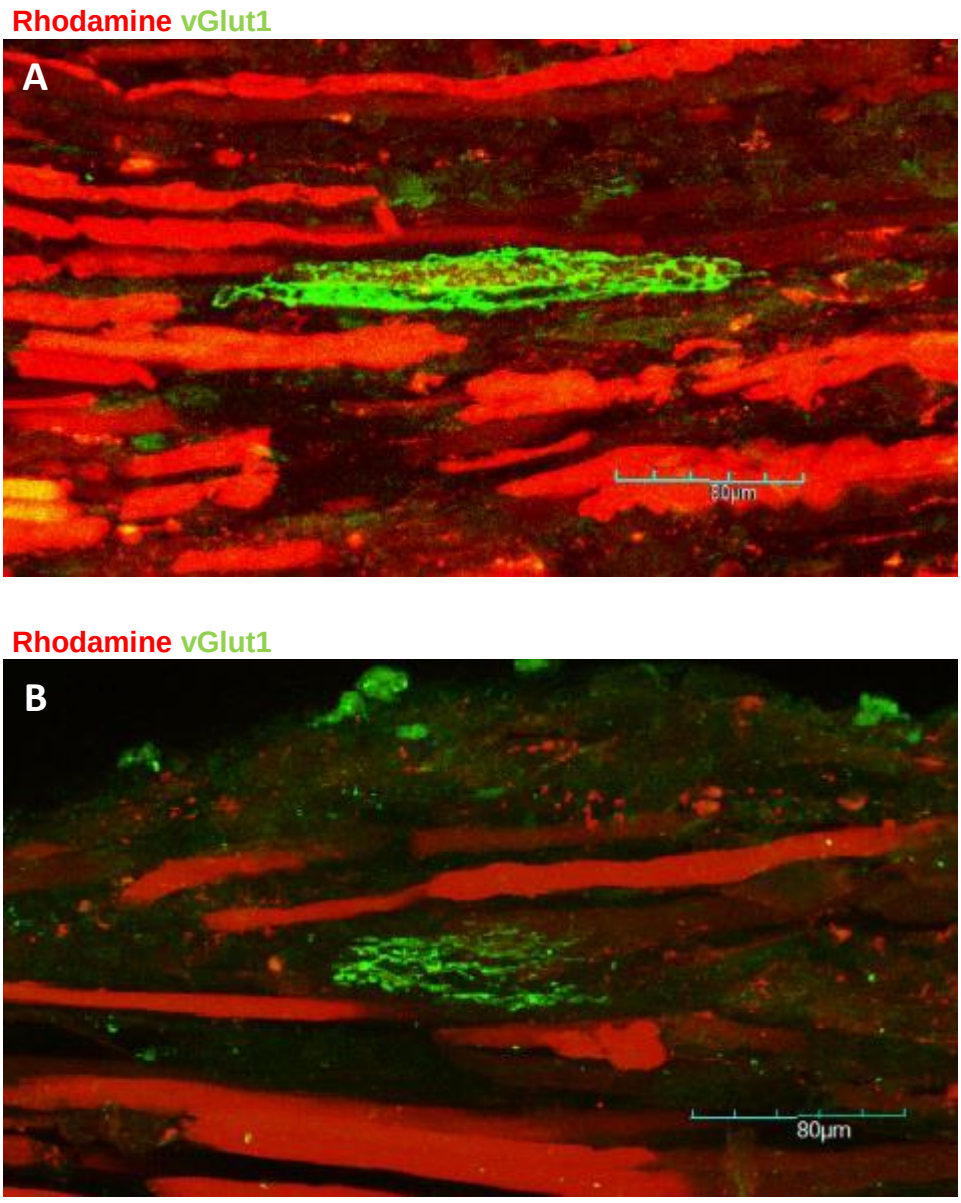

Figure 1: *Ex Vivo* Rhodamine Muscle Injection: MS vs GTO Confocal Images. Confocal images of muscle spindles (top) and Golgi tendon organs (bottom). (A) Longitudinal section through a muscle spindle labeled with rhodamine (red) and vGlut1 (green). Muscle fiber associated with the muscle spindle nerve terminal is labeled with the

rhodamine dye. The surrounding intrafusal muscle fibers display bright red rhodamine dye. (B) Golgi tendon organ sectioned longitudinally is labeled with vGlut1 (green). GTO is wrapped around a muscle fiber that lacks rhodamine dye (red). The surrounding muscle is inconsistently labeled red.

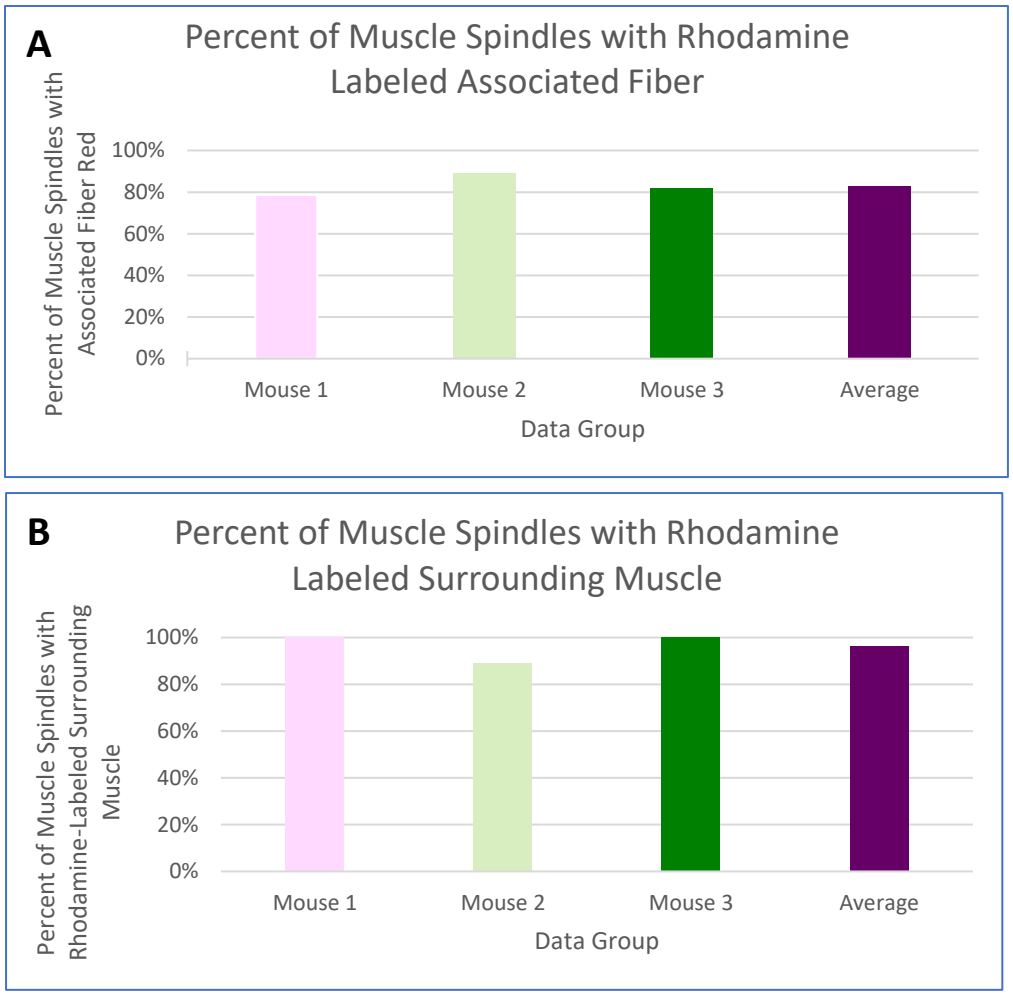

Figure 2: *Ex Vivo* Muscle Injection: MS Association with Rhodamine Dye Distribution. Muscle spindle nerve endings are associated with the area of the muscle affected by the rhodamine dye. (A) Percent of muscle spindles that are associated with a rhodamine-labeled muscle fiber. In mouse 1, 78.6% of muscle spindles are associated with a rhodamine-labeled muscle fiber, and 88.9% of muscle spindles in mouse 2 are associated with a rhodamine-labeled muscle fiber. The percent of muscle spindles in mouse 3 associated with a rhodamine-labeled muscle fiber is 81.8%, and the average between all 3

animals is 83.1%. (B) Percent of muscle spindles located in an area where the surrounding muscle is dyed red. All the muscle spindles in mouse 1 and mouse 3 (100%) were in an area where the surrounding muscle is rhodamine labeled. 89% of spindles were surrounded by red muscle fibers in mouse 2, and the average between the three mice is 96%.

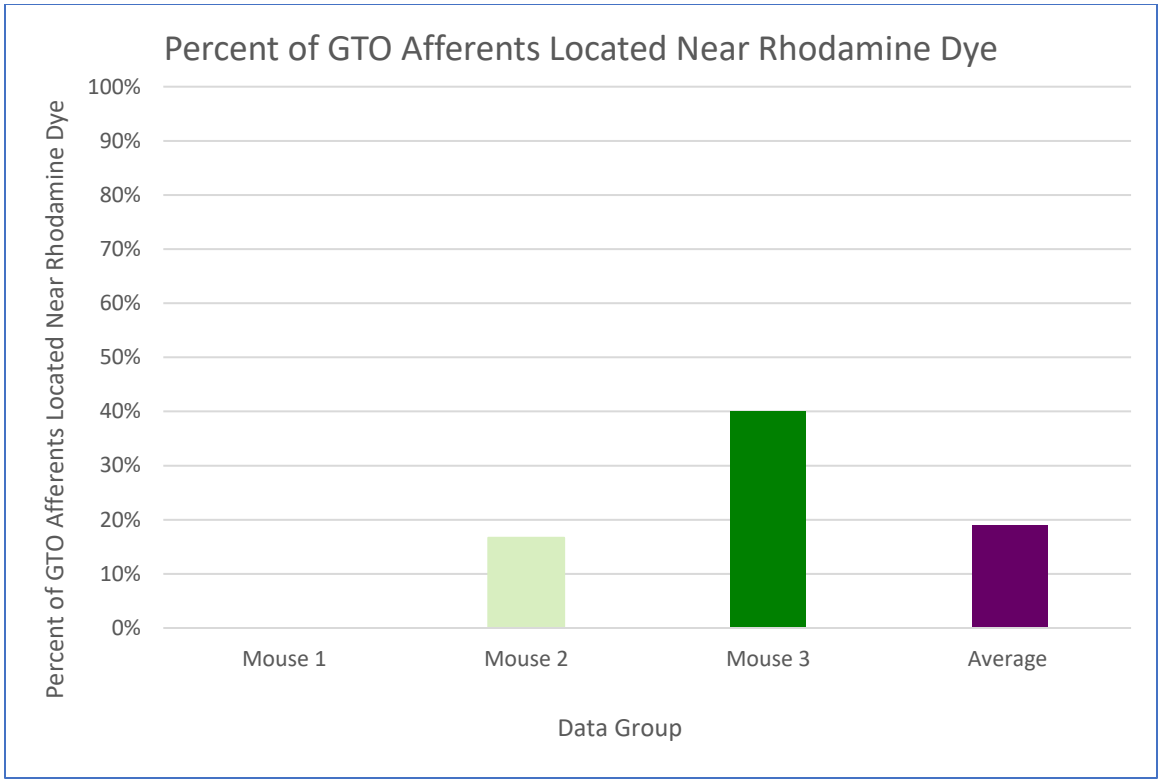

Figure 3: *Ex Vivo* Rhodamine Muscle Injection: Percent of GTO Afferents Association with Rhodamine Dye. Mouse 1 did not display any GTO afferents. Mouse 2 had 1 GTO (out of 6 total) that was located where the surrounding tissue had taken up the rhodamine dye (17%). 2 out of 5 GTO afferents in Mouse 3 were located near tissue with rhodamine dye (40%). On average, only 19% of identified GTOs were located near tissues with rhodamine dye.

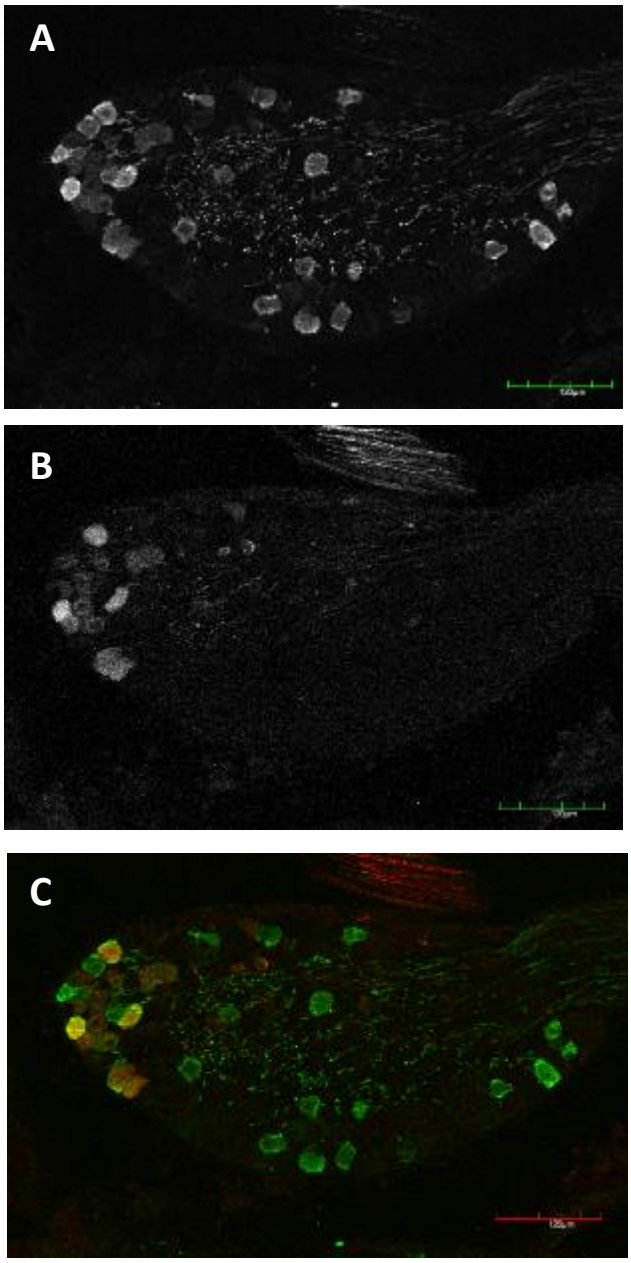

Figure 4: *Ex Vivo* Sciatic Nerve Backfills: Confocal images of Fluorescence L4 DRG PV/Rhodamine Labeled. (A) Alexa488 (green) channel only shows PV+ cells. There are many PV+ cells (green). (B) Cy3 (red) channel only shows Rhod+ cells. There are no

visible Rhod+ only cells. (C) Merged channels of Alexa488 and Cy3 show the double-labeled cells (PV+/Rhod+). There are approximately 70 double-labeled cells (PV+/Rhod+). Scale bar = 120 μm.

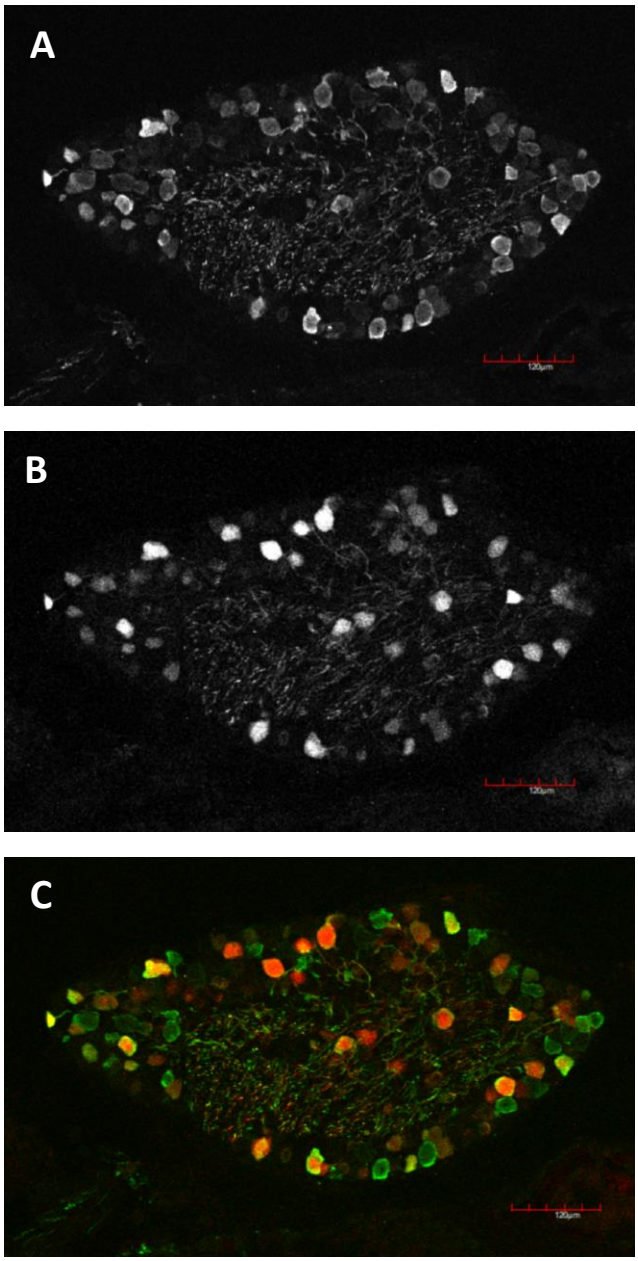

Figure 5: *Ex Vivo* Sciatic Nerve Backfills: Confocal images of Fluorescence L5 DRG PV/Rhodamine Labeled. (A) Alexa488 (green) channel only shows PV+ cells. (B) Cy3 (red) channel only shows Rhod+ cells. (C) Merged channels of Alexa488 and Cy3 show

the double-labeled cells (PV+/Rhod+). The L5 DRG has a more diverse profile of cells with approximately 184 green cells, 38 red cells, and 393 double-labeled cells. Scale bar = 120 μm.

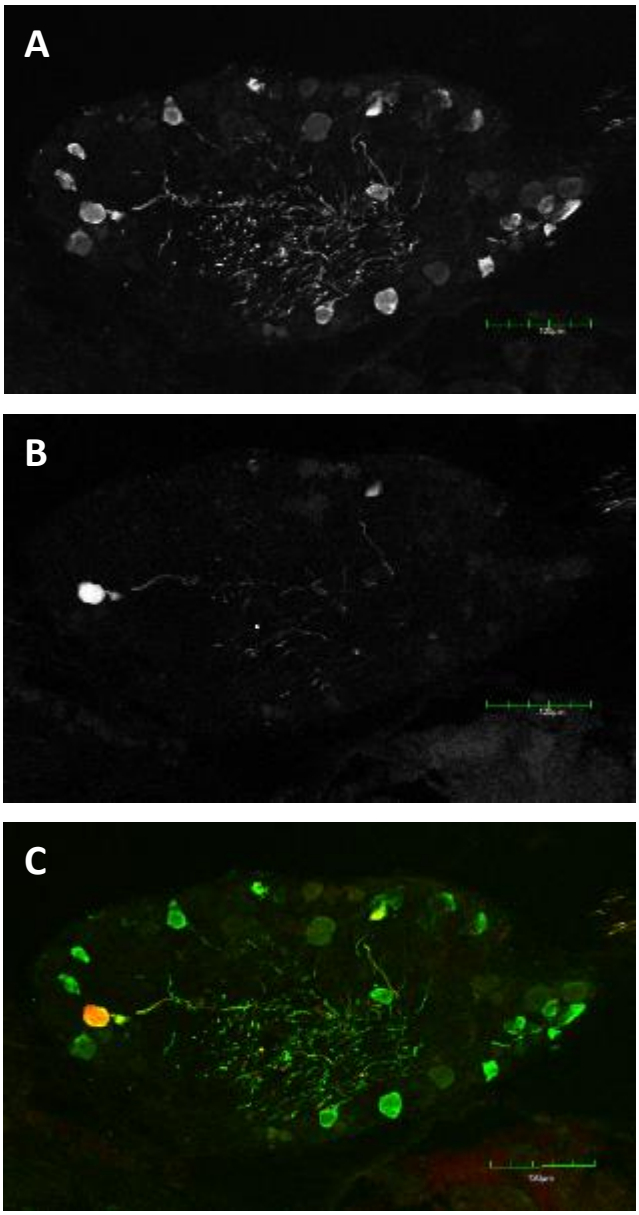

Figure 6: *Ex Vivo* Sciatic Nerve Backfills: Confocal images of Fluorescence L6 DRG PV/Rhodamine Labeled. (A) Alexa488 (green) channel only shows PV+ cells. There are many PV+ cells (green), particularly around the periphery of the DRG. (B) Cy3 (red) channel only shows Rhod+ cells. There are no visible Rhod+ only cells. (C) Merged

channels of Alexa488 and Cy3 show the double-labeled cells (PV+/Rhod+). There are many PV+ cells (green) and one double-labeled cell (PV+/Rhod+). Scale bar = 120 μm.

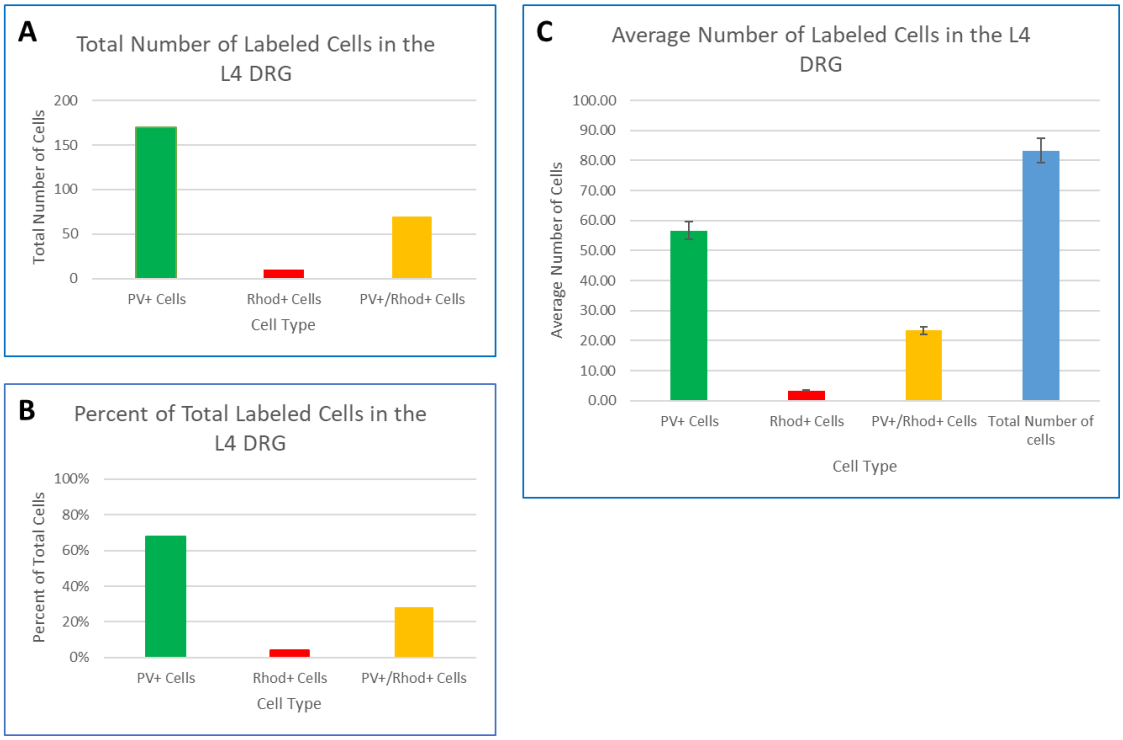

Figure 7: *Ex Vivo* Sciatic Nerve Backfills: Analysis of the L4 DRG. (A) The total number of cells at the L4 DRG level across animals 1, 2, 3, and 4. A total number of 170 PV+ cells, 10 Rhod+ Cells, and 70 PV+/Rhod+ (double-labeled) cells were analyzed. (B) The percent of each cell type compared to the total number of visible cells counted. 68% of cells are PV+ cells, 28% of cells are PV+/Rhod+ (double-labeled) cells, and only 4% of cells are Rhod+ cells. (C) The average number of each cell type in the L4 DRG between mouse 1, mouse 2, and mouse 3. On average, 56.67 PV+ cells, 3.33 Rhod+ cells, and 23.33 PV+/Rhod+ cells are located in the mouse DRG. The L4 DRG has an average of 83.33 labeled cells.

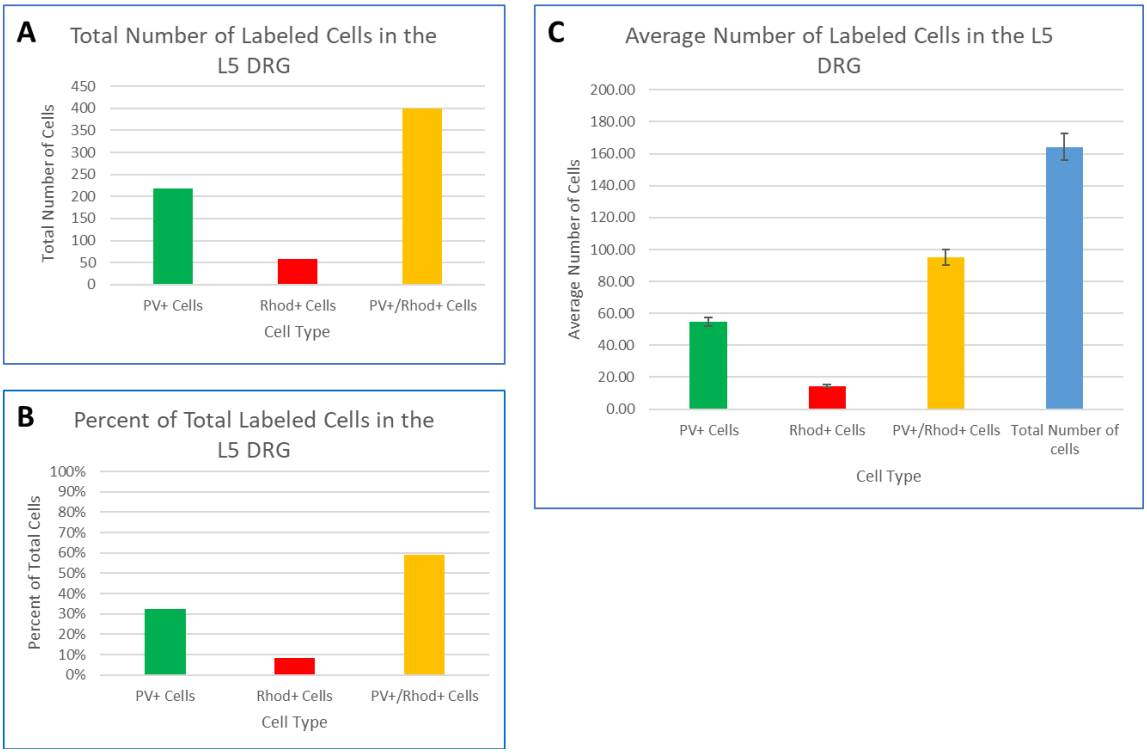

Figure 8: *Ex Vivo* Sciatic Nerve Backfills: Analysis of the L5 DRG. (A) The total number of 677 cells at the L5 DRG level across animals 1, 2, 3, and 4. A total number of 219 PV+ cells, 58 Rhod+ Cells, and 400 PV+/Rhod+ (double-labeled) cells were analyzed. (B) The percent of each cell type compared to the total number of visible cells counted. 32.35% of cells are PV+ cells, 59.08% of cells are PV+/Rhod+ (double-labeled) cells, and only 9% of cells are Rhod+ cells. (C) The average number of each cell type in the L5 DRG between mouse 1, mouse 2, and mouse 3. On average, 54.75 PV+ cells, 14.5 Rhod+ cells, and 95.0 PV+/Rhod+ cells are located in the mouse DRG. The L5 DRG has an average of 164.25 labeled cells.

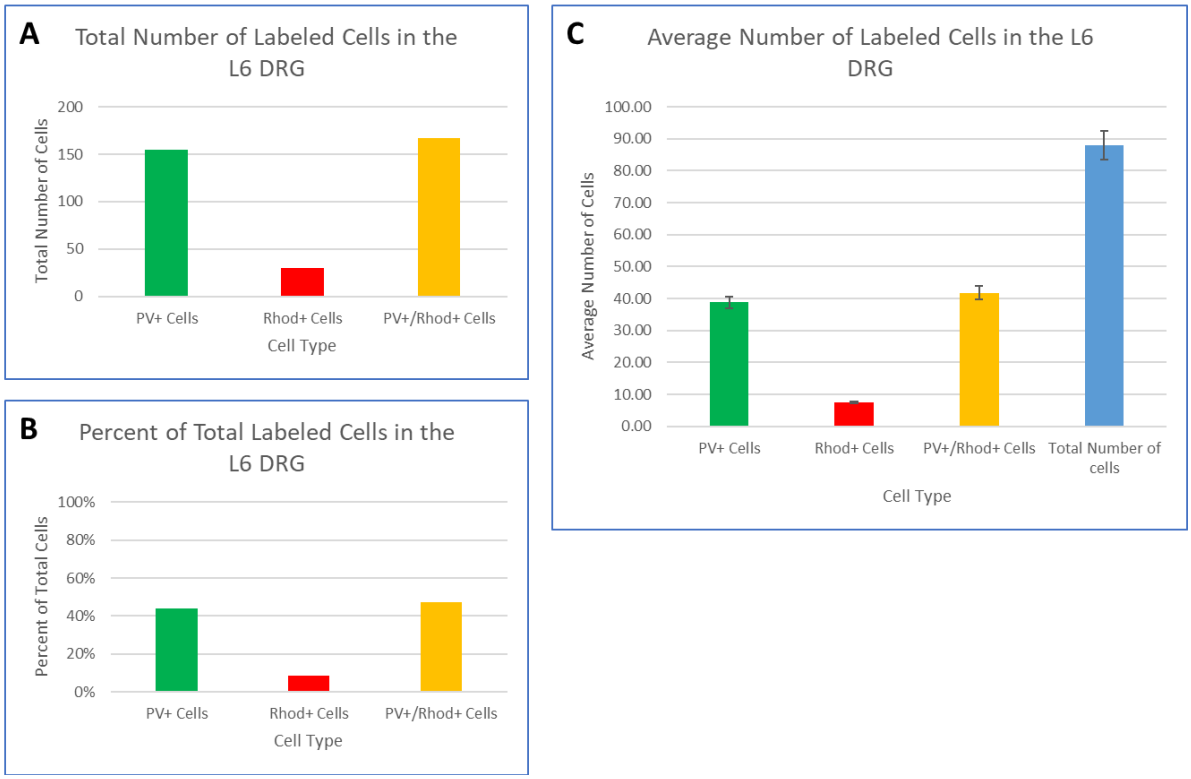

Figure 9: *Ex Vivo* Sciatic Nerve Backfills: Analysis of the L6 DRG. (A) The total number of 212 cells at the L6 DRG level across animals 1, 2, 3, and 4. A total number of 155 PV+ cells, 30 Rhod+ Cells, and 167 PV+/Rhod+ (double-labeled) cells were analyzed. (B) The percent of each cell type compared to the total number of visible cells counted. 44.03% of cells are PV+ cells, 47.44% of cells are PV+/Rhod+ (double-labeled) cells, and 8.52% are Rhod+ cells. (C) The average number of each cell type in the L6 DRG between mouse 1, mouse 2, and mouse 3. On average, 38.75 PV+ cells, 7.5 Rhod+ cells, and 41.75 PV+/Rhod+ cells are located in the mouse DRG. The L6 DRG has an average of 88.0 labeled cells.

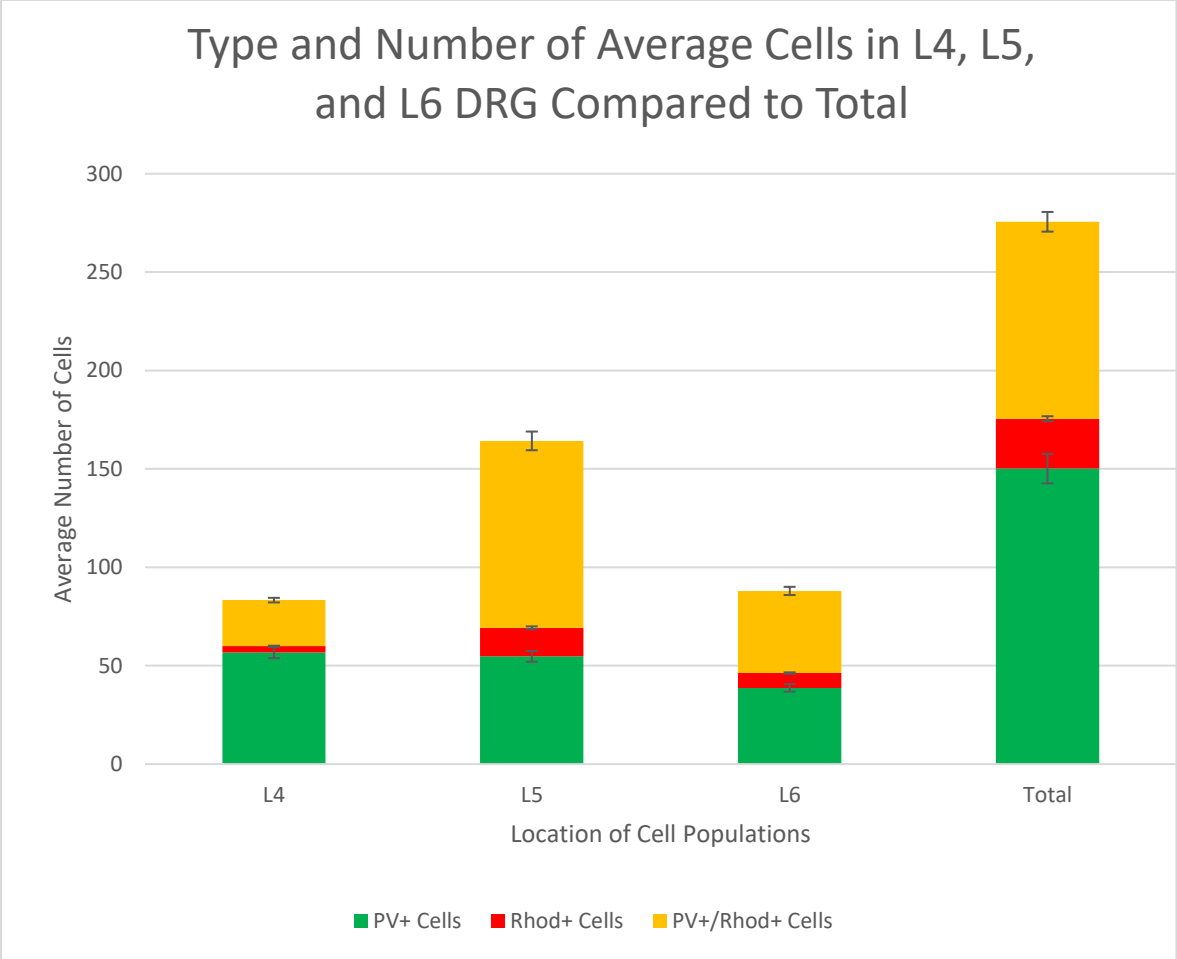

Figure 10: *Ex Vivo* Sciatic Nerve Backfills: Analysis of the Average Number of Each Cell Types in L4, L5, and L6 DRG. The L5 DRG has the most labeled cells with an average of 54.75 PV+ cells, 14.5 Rhod+ cells, and 95 PV+/Rhod+ (double-labeled) cells. The L4 DRG contained an average of 56.67 PV+ cells, 3.33 Rhod+ cells, and 23.33 double-labeled cells. The L6 DRG had an average of 38.75 PV+ cells, 7.5 Rhod+ cells, and 41.75 double-labeled cells. Across all the DRGs, there was an average total of 150.17 PV+ cells, 25.33 Rhod+ cells, and 100.08 double-labeled cells.

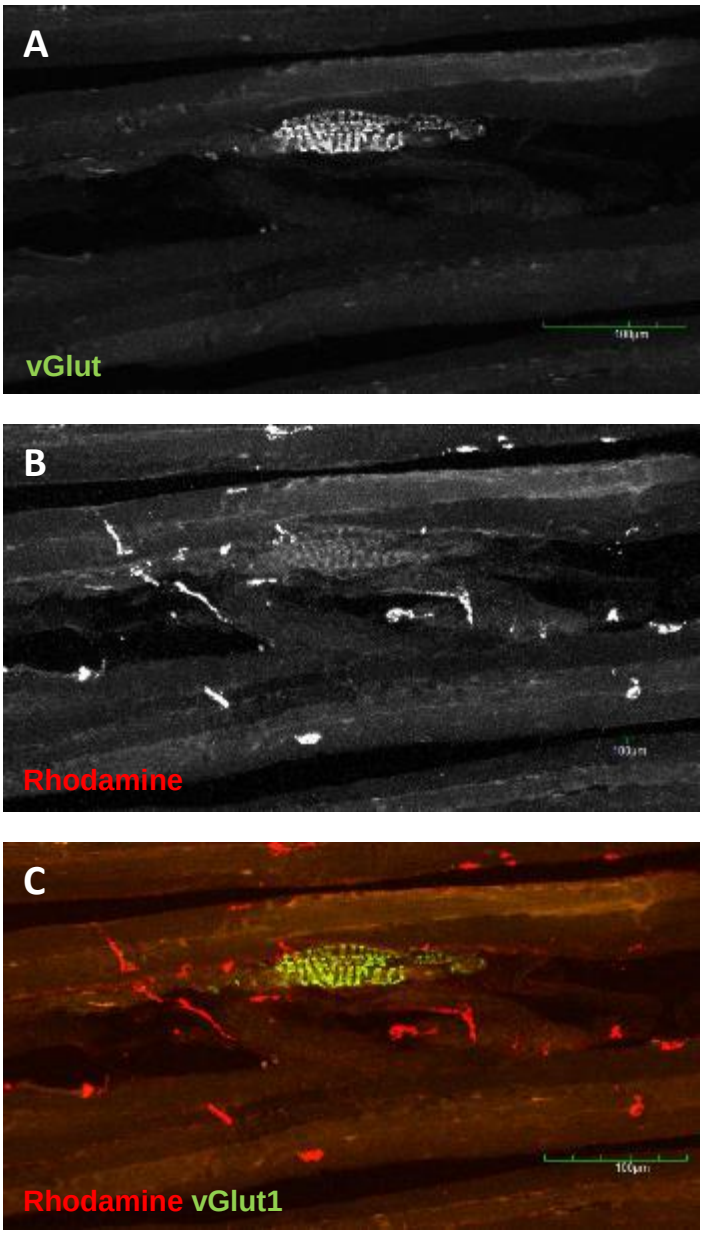

Figure 11: *In Vivo* Rhodamine Muscle Injections: Confocal Images of an MS Afferent. (A) Alexa 488 (green) channel only shows vGLUT1 labeled tissue. The muscle spindle afferent is visible and prominent in the green channel. (B) Cy3 (red) channel shows

tissues that contain Rhodamine dextran dye (Rhod+). The muscle spindle morphology is visible in this channel. (C) Combined channels (Alexa 488 and Cy3) show the MS's association with surrounding red muscle fibers. Scale bar = 100 μm.

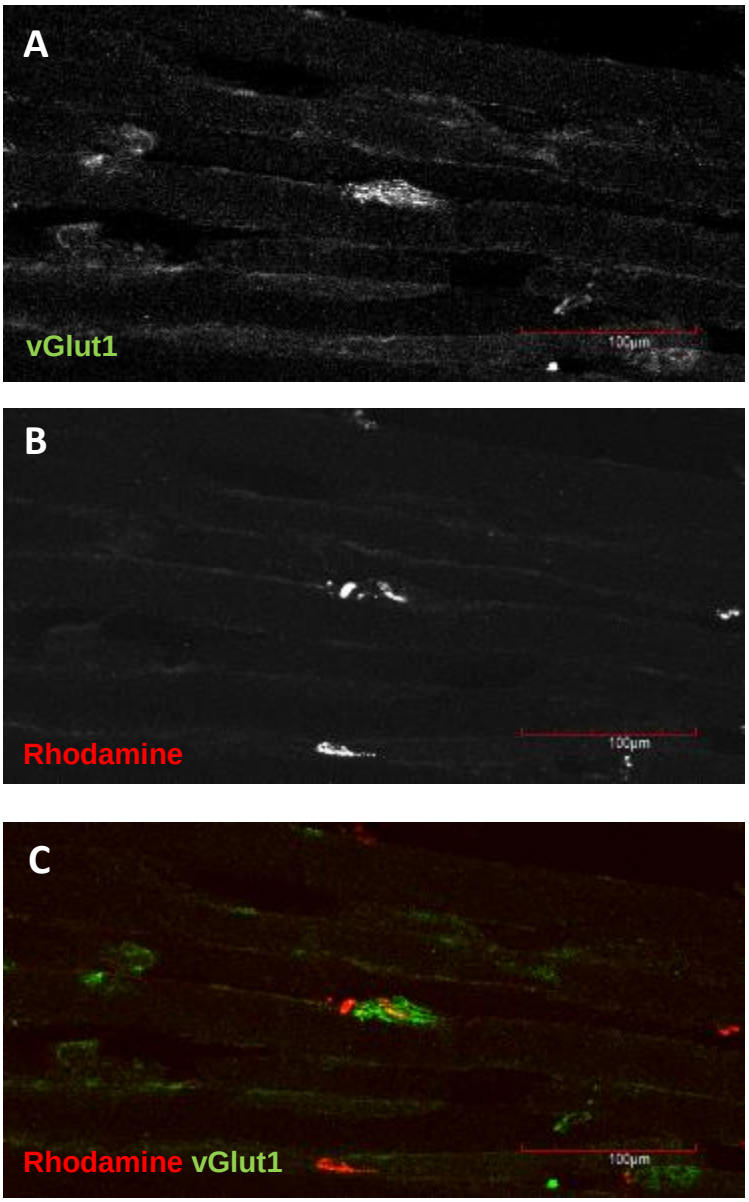

Figure 12: *In Vivo* Rhodamine Muscle Injections: Confocal Images of a GTO Afferent. (A) Alexa 488 (green) channel in grayscale shows vGLUT1 labeled tissue. The GTO afferent is visible in the green channel. (B) Cy3 (red) channel in grayscale shows tissues that contain Rhodamine dextran dye (Rhod+). The GTO afferent is not in this channel.

(C) Combined channels (Alexa 488 and Cy3) show the association of the GTO afferent with surrounding tissue and the distribution of Rhodamine dye. Scale bar = 100 μm.

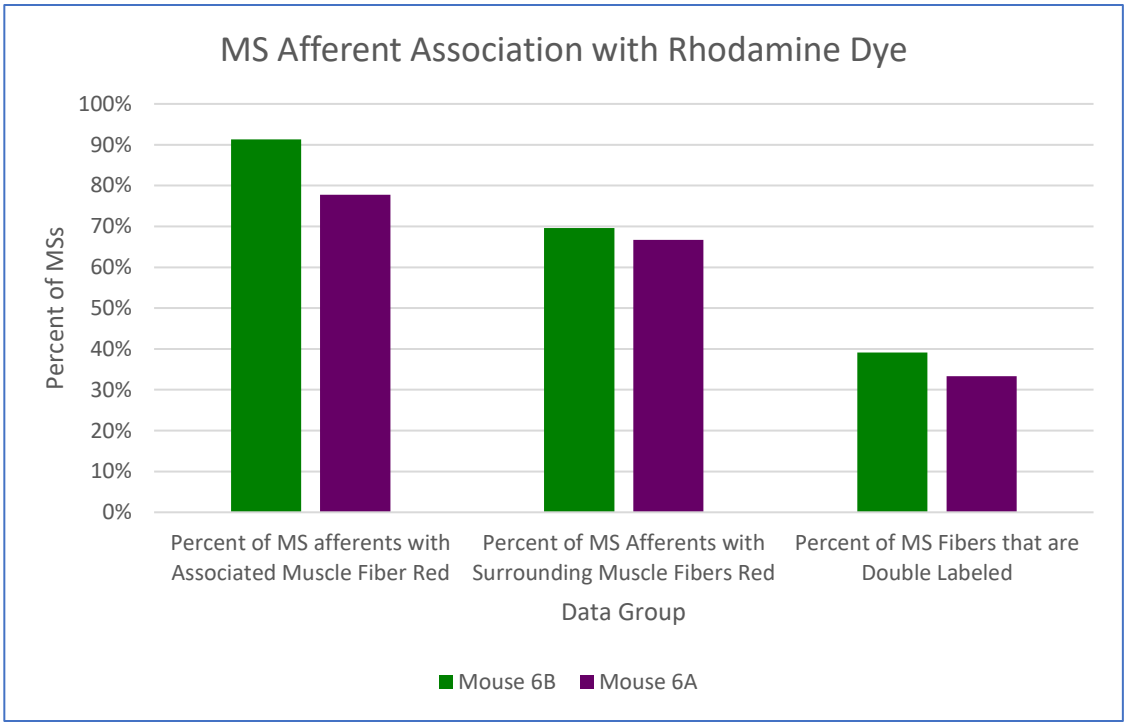

Figure 13: *In Vivo* Rhodamine Muscle Injection: MS Afferent Association with Rhodamine Dye. In Mouse 6B, 91.3% of MS afferents were wrapped around a red (rhodamine dyed) muscle fiber, 69.57% of MS afferents were located in an area where surrounding muscle fibers are red, and 39.13% of MS afferents were double-labeled. In Mouse 6A, 77.78% of MS afferents were associated with a red muscle fiber, 66.67% of MS afferents were located near red surrounding muscle fibers, and 33.33% of MS afferents are double-labeeld.

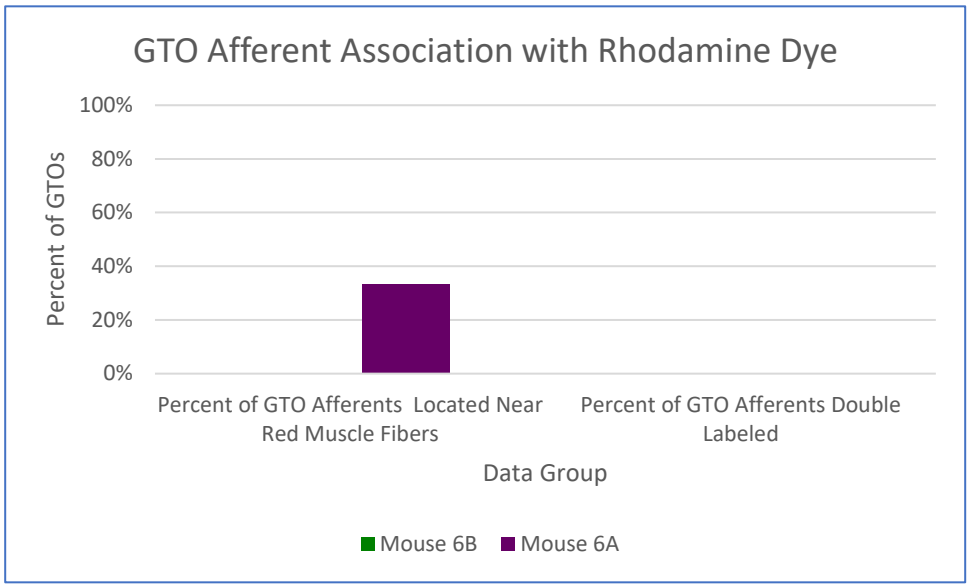

Figure 14: *In Vivo* Rhodamine Muscle Injection: GTO Afferent Association with Rhodamine Dye. None of the 5 total GTO afferents imaged were double-labeled (0% for both Mouse 6A and Mouse 6B). For Mouse 6B, no GTO afferents were located near any red (rhodamine-dyed) tissue (0%). For Mouse 6A, one GTO afferent (33.33%) was located near red muscle fibers.

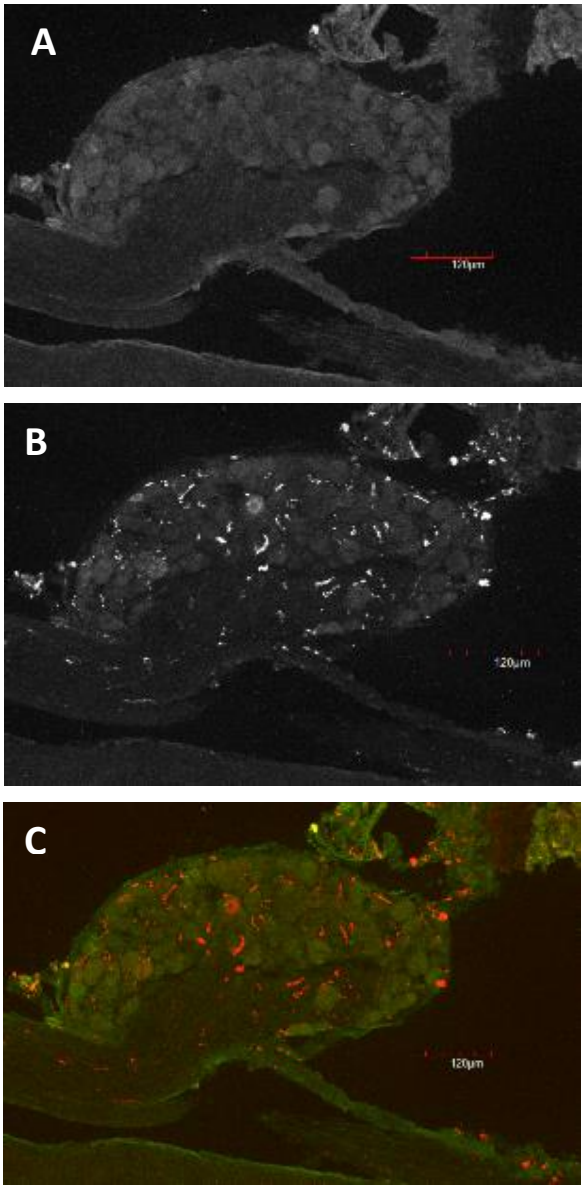

Figure 15: *In Vivo* Rhodamine Muscle Injection: Confocal Image of the L3 DRG. (A) Grayscale of the Alexa 488 (green) channel shows PV+ cells. (B) Grayscale of the Cy3 (red) channel shows Rhod+ cells. (C) Combined channels show PV+ cells, Rhod+ cells, and double-labeled cells. Scale bar = 120 μm.

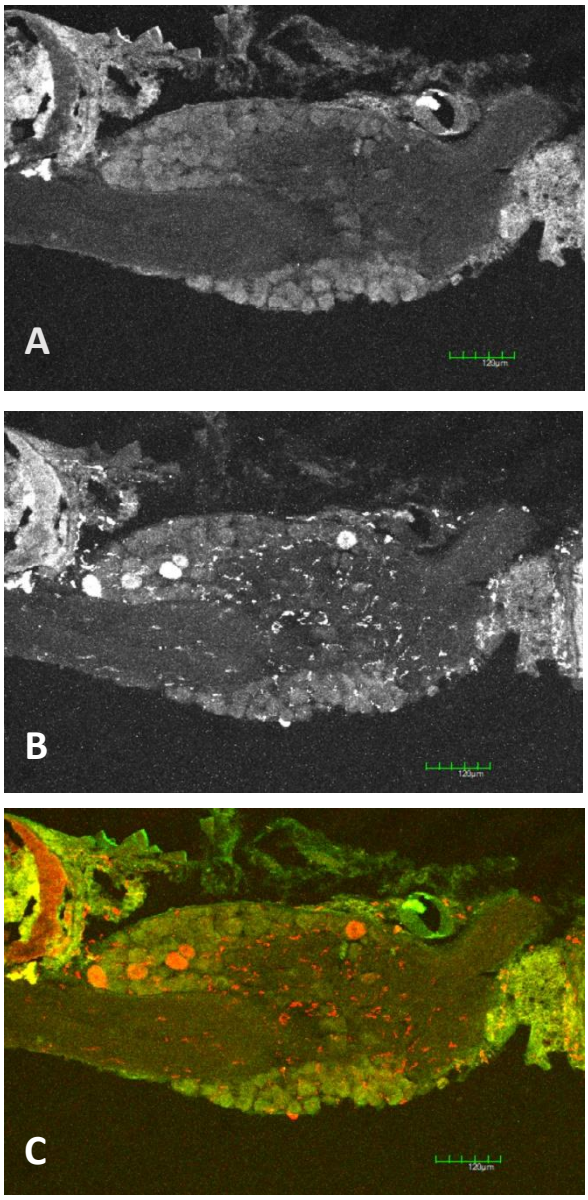

Figure 16: *In Vivo* Rhodamine Muscle Injection: Confocal Image of the L4 DRG. (A) Grayscale of the Alexa 488 (green) channel shows PV+ cells. (B) Grayscale of the Cy3 (red) channel shows Rhod+ cells. (C) Combined channels show PV+ cells, Rhod+ cells, and double-labeled cells. Scale bar = 120 μm.

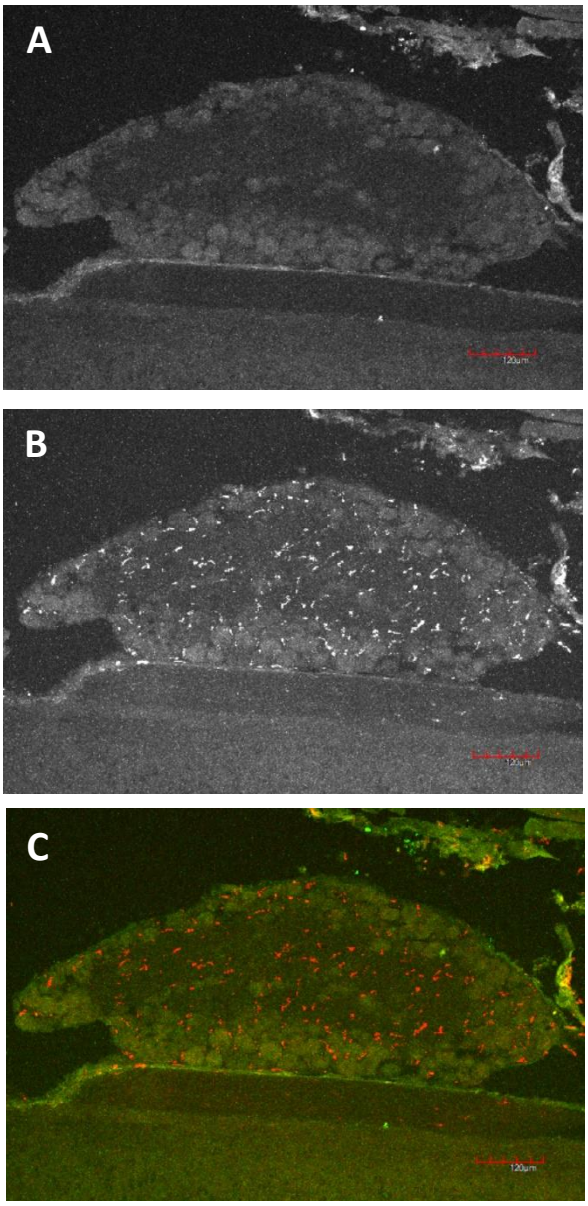

Figure 17: *In Vivo* Rhodamine Muscle Injection: Confocal Image of the L5 DRG. (A) Grayscale of the Alexa 488 (green) channel shows PV+ cells. (B) Grayscale of the Cy3 (red) channel shows Rhod+ cells. (C) Combined channels show PV+ cells, Rhod+ cells, and double-labeled cells. Scale bar = 120 μm.

Figure 18: *In Vivo* Rhodamine Muscle Injections: Analysis of the L3 DRG. (A) Mouse 6B had total of 25 PV+ cells, 1 Rhod+ cell, and 41 PV+/Rhod+ (double-labeled) cells in the L3 DRG. Mouse 6A displayed 9 PV+ cells, no Rhod+ cells, and 5 double-labeled cells. (B) In Mouse 6B, PV+ cells made up 37.31% of total cells, Rhod+ cells made up 1.49 % of total cells, and double-labeled cells made up 61.19% of total cells. In Mouse 6A, PV+ cells made up 64.29% of cells and double-labeled cells made up 35.71% of the total cell population. (C) The average number of cell types in the mouse L3 DRG. Between Mouse 6A and 6B, there was an average of 17 PV+ cells, 0.5 Rhod+ cells, and 23 double-labeled cells in the L3 DRG.

Figure 19: *In Vivo* Rhodamine Muscle Injections: Analysis of the L4 DRG. (A) Mouse 6B had total of 23 PV+ cells, 1 Rhod+ cell, and 19 PV+/Rhod+ (double-labeled) cells in the L4 DRG. Mouse 6A displayed 32 PV+ cells, 1 Rhod+ cell, and 6 double-labeled cells. (B) In Mouse 6B, PV+ cells made up 53.49% of the total cells, Rhod+ cells made up 3.32% of total cells, and double-labeled cells made up 44.19% of total cells. In Mouse 6A, PV+ cells made up 82.05% of cells, Rhod+ cells made up 2.56% of cells, and double-labeled cells made up 15.38% of the total cell population. (C) The average number of cell types in the mouse L4 DRG. Between Mouse 6A and 6B, there was an average of 27.50 PV+ cells, 1 Rhod+ cell, and 12.5 double-labeled cells in the L4 DRG.

Figure 20: *In Vivo* Rhodamine Muscle Injections: Analysis of the L5 DRG. (A) Mouse 6B had total of 14 PV+ cells, no Rhod+ cells, and 8 PV+/Rhod+ (double-labeled) cells in the L5 DRG. Mouse 6A displayed 12 PV+ cells, no Rhod+ cells, and 10 double-labeled cells. (B) In Mouse 6B, PV+ cells made up 63.63% of the total cells and double-labeled cells made up 36.36% of the total cells. In Mouse 6A, PV+ cells made up 54.54% of cells and double-labeled cells made up 45.45% of the total cell population. (C) The average number of cell types in the mouse L5 DRG. Between Mouse 6A and 6B, there was an average of 13 PV+ cells, no Rhod+ cells, and 9 double-labeled cells in the L5 DRG.

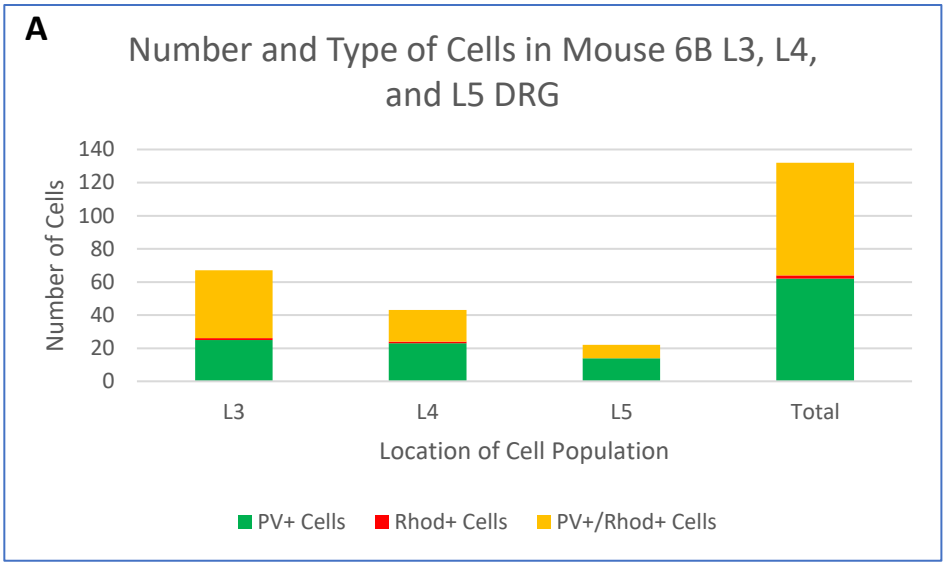

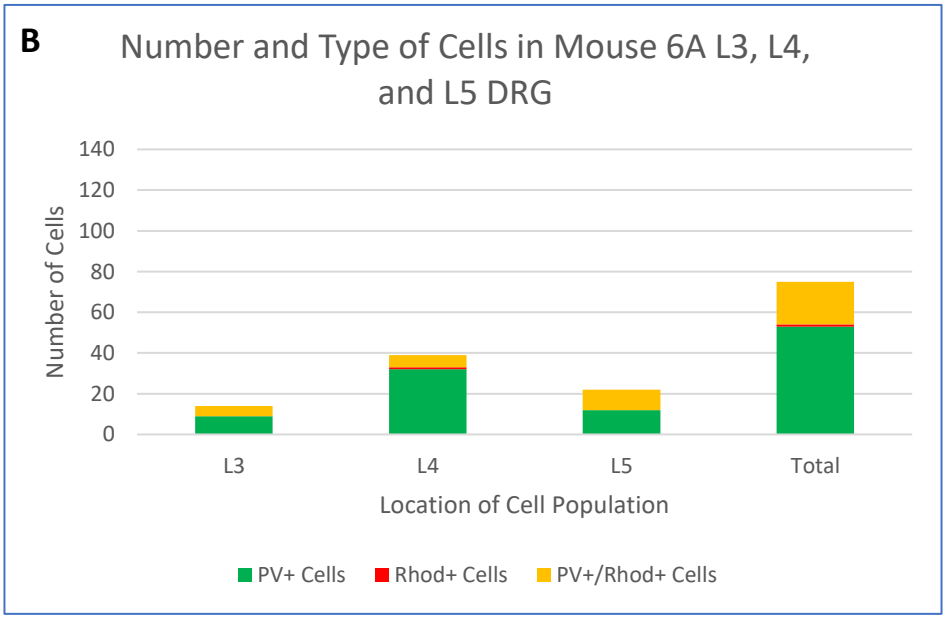

Figure 21: *In Vivo* Rhodamine Muscle Injection: DRG Cell Analysis for Mouse 6B and Mouse 6A. (A) Distribution of cell types in Mouse 6B L3, L4, and L5 DRGs. The L3 DRG in mouse 6B had 25 PV+ cells, 1 Rhod+ cell, and 41 double-labeled cells. The L4 DRG in mouse 6B had 23 PV+ cells, 1 Rhod+ cell, and 19 double-labeled cells. The L5

DRG in mouse 6B had the least number of cells, with no Rhod+ cells, 14 PV+ cells, and 8 double-labeled cells. (B) Distribution of cells in mouse 6A L3, L4, and L5 DRGs. The L3 DRG in mouse 6A had 9 PV+ cells, no Rhod+ cells, and 5 double-labeled cells. The L4 DRG had more cells, with 32 PV+ cells, 1 Rhod+ cell, and 6 double-labeled cells. Mouse 6A's L5 DRG exhibited 12 PV+ cells, no Rhod+ cells, and 10 double-labeled cells.

IV. Discussion

Ex Vivo Rhodamine Muscle Injections

Confocal microscopy of the rectus femoris muscle revealed that no proprioceptive structures (MSs or GTOs) were double labeled using the *ex vivo* animal preparation. However, a high percentage of muscle spindles images were associated with rhodamine-labeled muscle fibers (Figure 2A) and approximately 96% muscle spindles imaged had surrounding muscle labeled with the rhodamine dye (Figure 2B). This data indicated that it is possible for muscle spindles to take up rhodamine dye when it is injected directly into the target muscle. This lack of double labeling despite thorough distribution of the rhodamine dye could be due to complications in the *ex vivo* animal preparation, such as cells not receiving proper oxygenation. Consistent with previous studies, all GTOs imaged were located along the myotendinous boundaries of the muscle, where little to no rhodamine dye was injected (Schoultz and J.E., 1972). On average, only 19% of GTOs were located near muscle labeled with the rhodamine dye, and none were double labeled (Figure 3). Due to their differential location, MS afferents are likely to absorb the rhodamine dye when injected, but GTO afferents are not (Figure 1).

Ex Vivo Sciatic Backfills

To test the ability of sensory neurons to absorb and transport rhodamine dye to their cell bodies in the DRGs, rhodamine dye was backfilled into a fire-polished micropipette suctioned around the sciatic nerve, as previously described. The supporting DRGs (L4,

L5, and L6) were analyzed to quantify the number of proprioceptive afferents (PV+ cells), neurons projecting to the sciatic nerve (Rhod+ cells), and proprioceptive afferents that project to the sciatic nerve (double-labeled cells).

All three types of cells (PV+, Rhod+, and double-labeled) were observed in the L4 (Figure 4), L5 (Figure 5), and L6 (Figure 6) DRGs on the ipsilateral side of labeled sciatic nerve. This pattern of labeling suggests the successful transport of the rhodamine dye from the sciatic nerve to the associated DRGs. Figures 7 through 9 show the distribution and location of each labeled cell in the L4 through L6 DRGs. The L4 DRG contained mostly proprioceptive sensory neurons that did not project to the sciatic nerve, but also displayed non-pSN and pSN afferents that did project to the sciatic nerve. Double-labeled cells (pSNs that project to the sciatic nerve) were most abundant in the L5 DRG, but these cells were visible in the L4 through L6 DRGs (Figure 10). As shown in Figure 8 and 9, the L5 and L6 DRG exhibited labeled cells from all three categories (PV+, Rhod+, and PV+/Rhod+), but it is important to note that the majority of labeled cells in the L5 DRG are double labeled, indicating that most of proprioceptive sensory afferents in the L5 DRG project to the sciatic nerve. As shown in Figure 10, the L4, L5, and L6 DRGs exhibited cells labeled by the rhodamine dye and parvalbumin, which confirm the successful transport of the rhodamine dye to the supporting DRGs.

In Vivo Rhodamine Muscle Injections

To further evaluate the ability of rhodamine dye to selectively label muscle spindle afferents, the rhodamine dye was injected into the rectus femoris muscle *in vivo* as previously described. As shown in Figure 11, the muscle spindle is visible in the Cy3 channel, confirming the successful uptake of rhodamine dye into the muscle spindle afferents. Confocal analysis revealed that ~36.23% of MSs imaged were double-labeled, however ~84.54% of MSs were associated with rhodamine-dyed intrafusal muscle fibers. This suggests that there is room for improvement in the injection technique, particularly in the amount of rhodamine injected. Unfortunately, there were only a few GTO afferents identified; however, none were double-labeled and only one (an average of 16.67%) GTO was located near rhodamine-dyed tissue. This preliminary data suggests that MS afferents are labeled by the rhodamine dye injected into the muscle, while excluding GTO afferents. It is important to note that this technique can only distinguish between muscle spindle afferents (supplied by group Ia and group II endings) and Golgi tendon afferents (supplied by group Ib endings) and cannot distinguish between group Ia and group II endings.

Analysis of the L3, L4, and L5 DRGs, the DRGs that project to the femoral and quadriceps nerves revealed the successful transmission of the rhodamine dye from proprioceptive endings in the muscle to the DRGs. Three types of cells were quantified: proprioceptive cells that were not labeled by the rhodamine dye (PV+ cells), proprioceptive cells that project to the rectus femoris muscle and did transport the rhodamine dye (double-labeled cells), and cells that did transport the rhodamine dye but

are not proprioceptive afferents (Rhod+ cells). On average, the L3 and L4 DRGs had approximately the same number of labeled cells (~40.5 cells in the L3 and ~41 cells in the L4 DRG); however, the L4 DRG contained more PV+ cells and the L3 DRG contained more double-labeled cells. As shown in Figure 21, the *in vivo* rhodamine muscle injection was successful at labeling afferents that originate in the L3, L4, and L5 DRGs. From the lack of Rhod+ labeled cells (neurons that took up the rhodamine dye but are not proprioceptors), it can be concluded that the rhodamine injections favorably label proprioceptive afferents. However, few Rhod+ cells were observed in miniscule amounts compared to PV+ and double-labeled cells. Due to the small sample size, the comparison between survival times is inconclusive, and more studies are needed to further example the optimal survival time for this method.

While the *ex vivo* rhodamine muscle injection experiments did not produce any double-labeled proprioceptive afferents, it did show thorough and even rhodamine distribution within the rectus femoris muscle, which primarily surrounded MS afferents and not GTO afferents. This technique has the possibility to be successful; however, improvements in tissue oxygenation and survival are required. The *ex vivo* sciatic nerve backfill experiments displayed the capability of selectively labeling proprioceptive afferents in the DRGs of mice with the use of rhodamine dye. Finally, the *in vivo* rhodamine muscle injection experiments confirmed that by injecting rhodamine dye directly into the live rectus femoris muscle, it is possible to selectively label MS afferents in the corresponding DRGs. This technique has the potential to be used in *ex vivo* and *in*

vivo animal preparations and electrophysiology experiments where identifying and labeling proprioceptive subtypes is necessary.

V. References

Abdo H, Li L, Lallemend F, Bachy I, Xu X, Rice FL, Ernfors P (2011) Dependence on the transcription factor Shox2 for specification of sensory neurons conveying discriminative touch. Eur J Neurosci 34:1529–1541.

Arber S, Ladle DR, Lin JH, Frank E, Jessell TM, Hughes H (2000) ETS gene Er81 controls the formation of functional connections between group Ia sensory afferents and motor neurons. Cell 101:485–498.

Baldissera F, Hultborn H, Illert M (1981) Integration in spinal neuronal systems. In: Handbook of Physiology: The Nervous System (Brooks VB, ed), pp 509–595. American Physiology Society.

Banks RW (2005) The Muscle Spindle. In: Pheripheral neuropathy, 4th editio. (Dyck P, Thomas P, eds), pp 131–150. Philadelphia: WB Saunders.

Banks RW, Barker D, Stacey M. J. (1982) Form and distribution of sensory terminals in cat hindlimb muscle spindles. Philos Trans R Soc L B Biol Sci 299:329–364.

Barker D, Scott JJA, Stacey MJ, Scott H, Barker D, Road S (1985) Sensory reinnervation of cat peroneus brevis muscle spindles after nerve crush. Brain Res 333:131–138.

Blackmore M (2012) Molecular control of axon growth: insights from comparative gene profiling and high-throughput screening. Int Rev Neurobiol 105:39–70.

Blumer R, Konakci KZ, Brugger PC, Blumer MJF, Moser D, Schoefer C, Lukas JR,

Streicher J (2003) Muscle spindles and Golgi tendon organs in bovine calf extraocular muscle studied by means of double-fluorescent labeling, electron microscopy, and three-dimensional reconstruction. Exp Eye Res 77:447–462.

Boyd BYIA (1962) The structure and innervation of the nuclear bag muscle fibre system and the nuclear chain muscle fibre system in mammalian muscle spindles. Philos Trans R Soc B Biol Sci 245:81–87.

Brown BMC, Butler RG (1976) Regeneration of afferent and efferent fibres to muscle spindles after nerve injury in adult cats. J Physiol 260:253–266.

Chandran V, Coppola G, Nawabi H, Tuszynski M, Woolf CJ, Geschwind DH, Chandran V, Coppola G, Nawabi H, Omura T, Versano R, Huebner EA (2016) A systems-level analysis of the peripheral nerve intrinsic axonal growth program. Neuron 89:956–970 Available at: http://dx.doi.org/10.1016/j.neuron.2016.01.034.

Collins W, Mendell LM, Munson JB (1986) On the specificity of sensory reinnervation of cat skeletal muscle. J Physiol 375:587–609.

Crowe BYA, Matthews PBC (1964) The effects of stimulation of static and dynamic fusimotor fibres on the response to stretching of the primary endings of muscle spindles. J Physiol 174:109–131.

Davies P, Petit J, Scott JJA (1995) The dynamic response of Golgi tendon organs to tetanic contraction of in-series motor units. Brain Res 690:82–91.

De-doncker L, Picquet F, Petit J, Falempin M, Picquet F, Petit J (2003) Characterization of spindle afferents in rat soleus muscle using ramp-and-hold and sinusoidal stretches. J Neurophysiol 89:442–449.

de Nooij JC, Doobar S, Jessell TM (2013) Etv1 inactivation reveals proprioceptor subclasses that reflect the level of NT3 expression in muscle targets. Neuron 77:1055–1068 Available at: http://dx.doi.org/10.1016/j.neuron.2013.01.015.

Dun X, Parkinson DB (2018) Transection and crush models of nerve injury to measure repair and remyelination in peripheral nerve. In: Methods in Molecular Biology, pp 251–262.

Granit R (1975) The functional role of the muscle spindle - facts and hypotheses. Brain 98:531–556.

He Z, Jin Y (2016) Intrinsic control of axon regeneration. Neuron 90:437–451 Available at: http://dx.doi.org/10.1016/j.neuron.2016.04.022.

Hilton BJ, Bradke F (2017) Can injured adult CNS axons regenerate by recapitulating development? Development 144:3417–3429.

Hippenmeyer S, Shneider NA, Birchmeier C, Burden SJ, Jessell TM, Arber S (2002) A role for neuregulin1 signaling in muscle spindle differentiation. Neuron 36:1035–1049.

Houk J, Henneman E (1967) Responses of Golgi tendon organs to active contractions of

the soleus muscle of the cat. J Neurophysiol 30:466–481.

Hunt C, Louis S (1990) Mammalian muscle spindle: peripheral mechanisms. Physiol Rev 70:643–663.

Jami L (1992) Golgi tendon organs in mammalian skeletal muscle: functional properties and central actions. Physiol Rev 72:623–666.

Kamiyama XT, Kameda H, Murabe N, Fukuda S, Yoshioka N, Mizukami H, Ozawa K, Sakurai M (2015) Corticospinal tract development and spinal cord innervation differ between cervical and lumbar targets. J Neurosci 35:1181–1191.

Katz L, Iarovici D (1990) Green fluorescent latex microspheres: a new retrograde tracer. Neuroscience 34:511–520.

Katz LC, Burkhalter A, Dreyer WJ (1984) Fluorescent latex microspheres as a retrograde neuronal marker for in vivo and in vitro studies of visual cortex. Nature 310:498–500.

Kramer I, Sigrist M, Nooij JC De, Taniuchi I, Jessell TM, Arber S (2006) A role for Runx transcription Factor signaling in dorsal root ganglion sensory neuron diversification. Neuron 49:379–393.

Lallemend F, Ernfors P (2012) Molecular interactions underlying the specification of sensory neurons. Trends Neurosci 35:373–381 Available at: http://dx.doi.org/10.1016/j.tins.2012.03.006.

Li L, Rutlin M, Abraira VE, Cassidy C, Kus L, Gong S, Jankowski MP, Luo W, Heintz N, Koerber HR, Woodbury CJ, Ginty DD (2011) The functional organization of cutaneous low-threshold mechanosensory neurons. Cell 147:1615–1627 Available at: http://dx.doi.org/10.1016/j.cell.2011.11.027.

Ma Q, Fode C, Guillemot F, Anderson DJ (1999) Neurogenin1 and neurogenin2 control two distinct waves of neurogenesis in developing dorsal root ganglia. Genes Dev 13:1717–1728.

Matthews PB (1964) Muscle spindles and their motor control. Physiology 44:219–288.

Matthews PB (1981) Evolving views on the internal operation and functional role of the muscle spindle. J Physiol 320:1–30.

Odagaki K, Kameda H, Hayashi T (2018) Mediolateral and dorsoventral projection patterns of cutaneous afferents within transverse planes of the mouse spinal dorsal horn. J Comp Neurol 527:972–984.

Oliver KM, Florez-Paz DM, Badea TC, Mentis GZ, Menon V, de Nooij JC (2021) Molecular correlates of muscle spindle and Golgi tendon organ afferents. Nat Commun 12 Available at: http://dx.doi.org/10.1038/s41467-021-21880-3.

Oscarsson O (1965) Functional organization of the spino- and cuneocerebellar tracts. Physiol Rev 45:495–522.

Poliak S, Norovich AL, Yamagata M, Sanes JR, Jessell TM (2016) Muscle-type identity

of proprioceptors specified by spatially restricted signals from limb mesenchyme. Cell 164:512–525 Available at: http://dx.doi.org/10.1016/j.cell.2015.12.049.

Renthal W, Tochitsky I, Yang L, Cheng YC, Li E, Kawaguchi R, Geschwind DH, Woolf CJ (2020) Transcriptional reprogramming of distinct peripheral sensory neuron subtypes after axonal injury. Neuron 108:128-144.e9 Available at: https://doi.org/10.1016/j.neuron.2020.07.026.

Schoultz TW, J.E. S (1972) The fine structure of the Golgi tendon organ. J.of Neurocytol 1:1–26.

Scott JJA (2005) The Golgi Tendon Organ. In: Peripheral neuropathy, 4th editio. (Dyck P, Thomas PK, eds), pp 151–161. Philadelphia: WB Saunders.

Sherrington CS (1884) On the anatomical constitution of nerves of skeletal muscles; with remarks on recurrent fibres in the ventralspinal nerve-root. J Physiol Lond 17:211–258.

Sherrington CS (1907) Strychnine and reflex inhibition of skeletal muscle. J Physiol 36:185–204.

Shrestha SS, Bannatyne BA, Jankowska E, Hammar I, Nilsson E, Maxwell DJ (2012) Excitatory inputs to four types of spinocerebellar tract neurons in the cat and the rat thoraco-lumbar spinal cord. J Physiol 590:1737–1755.

Sonner MJ, Walters MC, Ladle DR (2017) Analysis of proprioceptive sensory

innervation of the mouse soleus: A whole-mount muscle approach. PLoS One 12:1–18.

Tourtellotte WG, Milbrandt J (1998) Sensory ataxia and muscle spindle agenesis in mice lacking the transcription factor Egr3. Nat Genet 20:87–91.

Verdu E, Navarro X (1997) Comparison of immunohistochemical and functional reinnervation of skin and muscle after peripheral nerve injury. Exp Neurol 198:187–198.

Windhorst U (2007) Muscle proprioceptive feedback and spinal networks. Brain Res Bull 73:155–202.

Wu D, Schieren I, Qian Y, Zhang C, Jessell TM, De Nooij JC (2019) A role for sensory end organ-derived signals in regulating muscle spindle proprioceptor phenotype. J Neurosci 39:4252–4267.